Journal of Structural Geology 33 (2011) 1023–1043

Contents lists available at ScienceDirect

Journal of Structural Geology

journal homepage: www.elsevier.com/locate/jsg

The Eidsfjord shear zone, Lofoten–Vesterålen, north Norway: An Early Devonian, paleoseismogenic low-angle normal fault

Mark G. Steltenpohl [a,*], David Moecher [b], Arild Andresen [c], Jacob Ball [a], Stephanie Mager [d], Willis E. Hames [a]

[a] Department of Geology and Geography, Auburn University, Auburn, AL 36849, USA
[b] Department of Earth and Environmental Sciences, University of Kentucky, Lexington, KY 40506-0053, USA
[c] Department of Geosciences, University of Oslo, Box 1047, Blindern, Oslo 3, Norway
[d] Department of Earth Sciences, Indiana University and Purdue University Indianapolis, Indianapolis, IN 46202, USA

ARTICLE INFO

Article history:
Received 29 June 2010
Received in revised form
4 January 2011
Accepted 29 January 2011
Available online 22 February 2011

Keywords:
Detachments
Caledonian
Devonian extension
Lofoten–Vesterålen
Norway
Seismogenic fault
Muscovite $^{40}Ar/^{39}Ar$

ABSTRACT

We report structural and $^{40}Ar/^{39}Ar$ isotopic information on the Eidsfjord shear zone that document it to be a seismogenic, tops-west (hinterland directed), Devonian ductile low angle (25–30° dip, shallowing locally) normal detachment fault. Anorthosite/migmatitic gneiss in the detachment's upper plate, mangerite in the lower plate, and detachment mylonites are all cut by generations of abundant pseudotachylyte occurring over approximately 150 km^2. The mean of four laser $^{40}Ar/^{39}Ar$ plateau ages for single crystals of recrystallized muscovite from mylonites defining the Eidsfjord shear zone indicates an age of 403.6 ± 1.1 Ma (2σ) for deformation and recrystallization. $^{40}Ar/^{39}Ar$ step-heating analyses are reported for muscovite from mylonitized rocks of the Fiskefjord shear zone, a nearby tops-east Caledonian thrust that was reactivated as a tops-west normal fault, documenting cooling of the upper plate through the ~350 °C isotherm at ~457 Ma. Together with Middle-Ordovician tectonothermal relics found farther west in Lofoten, tops-down-to-the-west normal-slip movement on these extensional shear zones explains maintenance of high-crustal levels throughout the Siluro-Devonian Scandian event. Potassium feldspar $^{40}Ar/^{39}Ar$ results document a pulse, or multiple pulses, of uplift and cooling between ca. 235 Ma and 185 Ma, consistent with formation of Triassic–Jurassic rift basins flanking the Lofoten Ridge.

The Eidsfjord detachment appears to mark the northern terminus of the Early Devonian detachment system traceable 800 km southward to the Nordfjord–Sogn detachment and westward across the North Atlantic to detachments of roughly the same age on the conjugate side of the orogen in East Greenland. The timing, geometry, kinematics, and rheological development of Eidsfjord detachment are grossly similar to the Nordfjord–Sogn detachment but the former contrasts in that it presently lacks exposed deposits of Devonian sedimentary rocks, has smaller magnitudes of displacement, a more prolonged exhumation history, is severely chopped by later high angle normal faults related to rifting and final Eocene continental separation, and it has abundant pseudotachylite occurrences in the upper plate. We interpret the Eidsfjord detachment to be a rare example of an ancient eroded seismogenic low-angle normal fault.

1. Introduction

The Nordfjord–Sogn detachment fault in the Western Gneiss Region of west Norway (Fig. 1) is perhaps Earth's best exposed and accessible example of extreme magnitude and rapid tectonic exhumation along an ancient normal detachment system (Andersen and Jamtveit, 1990; Walsh et al., 2007). Large tracts of high- and ultrahigh-pressure (coesite- and diamond-bearing) eclogites in the Western Gneiss Region occur mainly in Precambrian continental basement of the Baltic Shield lower plate. Eclogitization of the footwall is interpreted to reflect Silurian-Early Devonian ("Scandian"; ca. 425-390 Ma) subduction of the western edge of Baltica beneath eastern Laurentia (Andersen and Jamtveit, 1990). Continental basement of the lower plate remained under ultra-high pressure conditions (≤40 kbar–120 km depth) well into the Early Devonian (400–390 Ma: Hacker et al., 2006) before being

* Corresponding author.
E-mail address: steltmg@auburn.edu (M.G. Steltenpohl).

0191-8141/$ – see front matter © 2011 Elsevier Ltd. All rights reserved.
doi:10.1016/j.jsg.2011.01.017

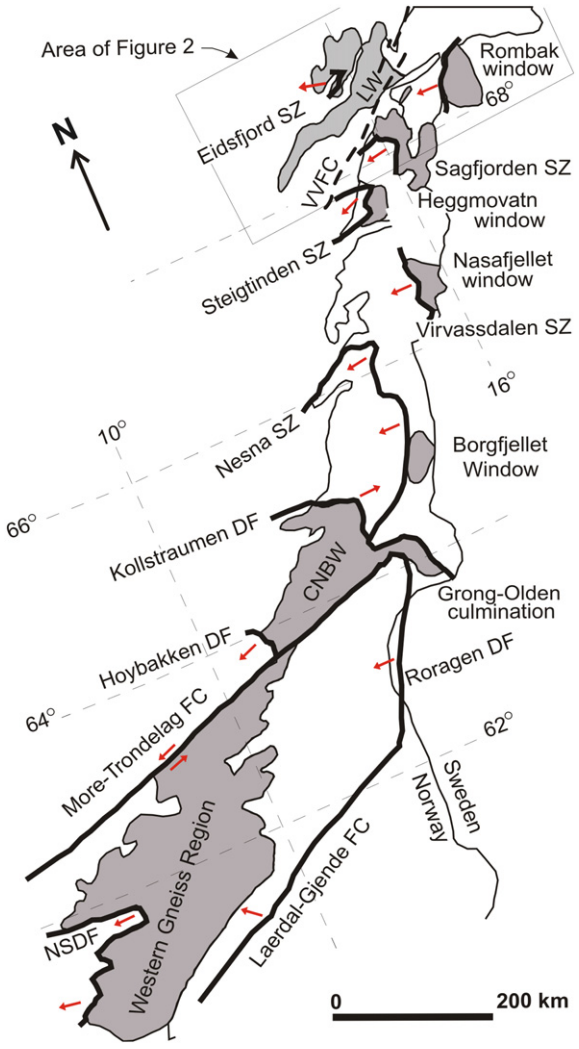

Fig. 1. Devonian extensional detachment system in the Norwegian Caledondies (modified from Braathen et al., 2002; Osmundsen et al., 2003, and Steltenpohl et al., 2009). Gray areas are lower plate, mostly Baltic basement windows. Red arrows indicate the predominant direction of extension. CNBW – Central Norwegian Basement Window, DF – Detachment Fault, FC – Fault Complex, LW – Lofoten window, NSDF – Nordfjord–Sogn detachment fault, SZ – Shear Zone, VVFC – Vanna-Vestfjord Fault Complex. (For interpretation of the references to colour in this figure legend, the reader is referred to the web version of this article.)

rapidly juxtaposed (~10 m.y.) with nonmetamorphosed Early Devonian strata in the upper plate. Seismic and potential field subsurface studies of the highly attenuated Norwegian continental margin have identified Mesozoic and Cenozoic low-angle normal detachment faults along which this deep crust was further exhumed, in the manner of a metamorphic core complex (Osmundsen and Ebbing, 2008). These detachments are proposed to reactivate the Devono-Carboniferous ductile faults that accommodated late-to-post-orogenic Caledonian extension.

In contrast to western Norway, Devonian sedimentary basins are not reported anywhere in north Norway, onshore or offshore, and structural and isotopic age data remain insufficient to verify whether Devonian extensional structures are preserved as far north as Lofoten–Vesterålen (Steltenpohl and Bartley, 1993; Steltenpohl et al., 2004). Workers have documented that the Devonian orogen-parallel extensional system extends several hundred kilometers northward from its type area in west Norway to the Nesna shear zone near the arctic circle (Fig. 1: Eide et al., 2002; Osmundsen et al., 2003). Far less-detailed geological information is available for the large area between the Nesna shear zone and Lofoten (Fig. 1), however, leaving its extrapolation northward less than certain. Similarities in the style and kinematics between the Nesna shear zone and shear zones that occur along the western margins of several basement windows farther north were used to infer that this extensional system continues an additional 400 km northward to the Rombak window (Fig. 1: Braathen et al., 2002; Eide et al., 2002; Osmundsen et al., 2003; Steltenpohl et al., 2009). The role of Devonian extension in the Lofoten-Rombak region (Fig. 2) remains the topic of debate because evidence for it remains largely inferential (Steltenpohl and Bartley, 1988, 1993; Rykkelid, 1992; Fossen and Rykkelid, 1992, 1993; Rykkelid and Andresen, 1994; Olesen et al., 2002; Wilson et al., 2006). Clarifying the extent of Devonian extension to the north in Scandinavia is critical for evaluating extensional processes that had operated along the entire length of this continent-scale system of detachments. Combined with a relatively straightforward palinspastic restoration that allows for its connection to that becoming better understood on the conjugate side of the orogen exposed in East Greenland make this an exceptional area in which to evaluate processes of continental extension (e.g.: Hartz and Andresen, 1995; Ebbing et al., 2006; Fossen, 2010).

Herein we report field, kinematic, and $^{40}Ar/^{39}Ar$ isotopic data documenting the discovery of a large area (~200 km^2) of the Lofoten-West Troms Basement Complex (Figs. 1 and 2), arctic Norway (68.5°N), affected by intense late- and-post Caledonian (Early Devonian and later) extensional deformation. A major topswest, Early Devonian low-angle normal detachment fault is herein referred to as the Eidsfjord shear zone.As will be shown, the Eidsfjord shear zone exhibits several core complex characteristics. In addition, the upper plate and structural levels within and immediately beneath the detachment contain generations of pseudotachylite, some of which are mylonitic and/or metamorphosed, implying a prolonged history of seismicity during normal faulting. We compare and contrast the Eidsfjord shear zone with extensional structures documented in central and southwest Norway, that in turn have general significance for models of continental extension immediately following continent–continent collision.

2. Stuctural analysis

Heier (1960) first reported a discontinuous shear zone along the southeast and northwest coast of Eidsfjord on Langøya in the Lofoten-West Troms basement window (Fig. 3). Løseth and Tveten (1996) mapped additional brittle and ductile faults southeast of Eidsfjord on western Hinnøya (Fig. 3), as part of Heier's shear zone. Archaean and Proterozoic continental basement rocks (anorthosite, mangerite, monzonite, and migmatite) in the window were metamorphosed under granulite- or upper-amphibolite-facies conditions at ~1.8–1.7 Ga (Griffin et al., 1978; Corfu, 2004). Despite its internal orogenic position and occurrence structurally beneath the stack of Caledonian allochthons that overrode it toward the east, Caledonian metamorphic and deformational effects in Lofoten are strictly limited to shear zones (Tull, 1978; Bartley, 1982; Hames and Andresen, 1996; Steltenpohl et al., 2004). The Lofoten window lies roughly along strike of the Western Gneiss Region (Fig. 1) and likewise is considered to be the western edge of Baltica (today's coordinates) that was deeply subducted beneath Laurentia during the Caledonian orogeny (Hodges et al., 1982; Steltenpohl et al., 2003b).

We investigated Heier's (1960) shear zone in detail on the southeast coast of Eidsfjord on the island of Langøya (Figs. 2 and 3), where we propose the type locality for the Eidsfjord shear zone. We also present preliminarily results on fault rocks and pseudotachylites exposed around Fiskefjord on western Hinnøya, where a more

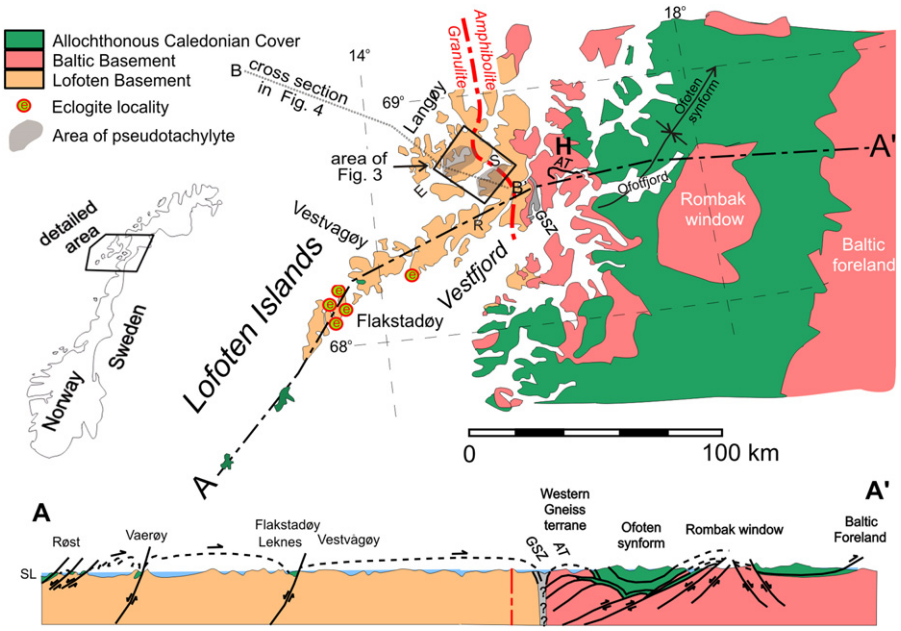

Fig. 2. Location map of the study area and simplified geologic cross section A–A′ (after Steltenpohl et al., 2006). Note locations of the area of Fig. 2 and trace of cross section B–B′ in Fig. 4.

cryptic and disjointed set of shears and faults are refered to as the Fiskefjord shear zone (also see Mager, 2005).

Ductile and brittle fault rocks associated with the Eidsfjord shear zone are best exposed along the southeast coast of Eidsfjord, with the main detachment exposed on Gjurtinden at Slåttnes and Grønning (Fig. 3). Mylonites in anorthosite and mangerite are also exposed discontinuously to the southwest end of Langøya near Kalsnes (Fig. 3). The Eidsfjord shear zone is a 200-m thick zone of mylonite capped by a brittle detachment surface displaying tops-down-to-the-west normal-slip movement (Figs. 4 and 5). The Precambrian (?) foliation observed in the country rock, S_1, is defined as an amphibolite-facies gneissosity and migmatitic

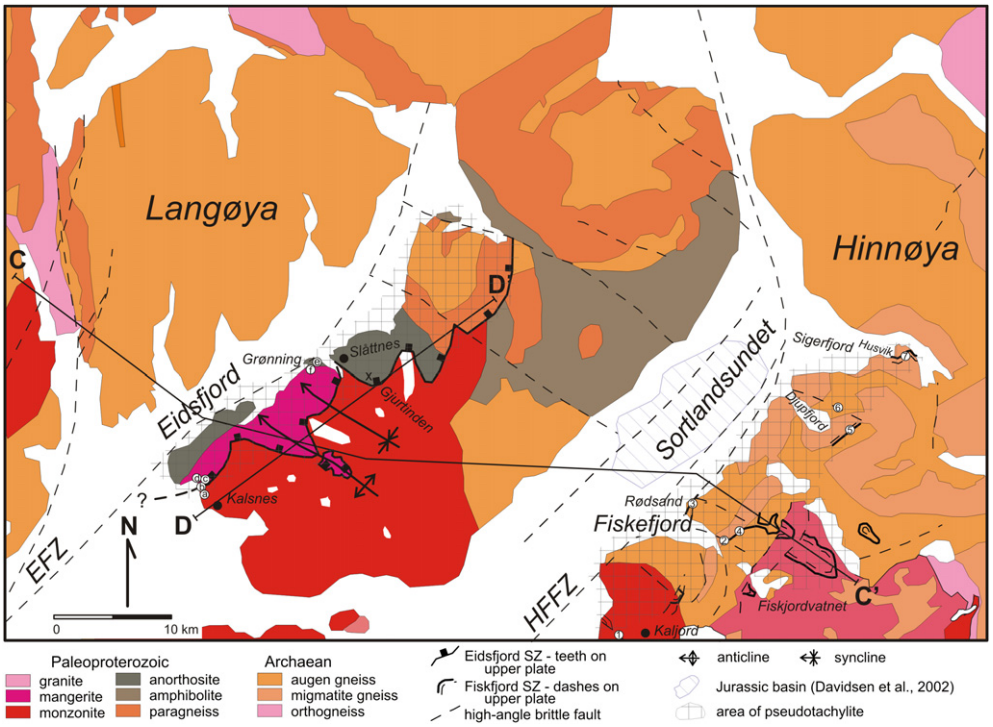

Fig. 3. Geologic map of the Eidsfjord and Fiskfjord shear zones and traces of geologic cross sections C–C′ (the southeast end of the onshore part of section B–B′ in Fig. 2) and D–D′ shown in Fig. 4 (after Steltenpohl et al., 2006). White circles with letters (Eidsfjord samples) and numbers (Fiskefjord samples) are localities for the $^{40}Ar/^{39}Ar$ isotopic analyses: a = TK07-37; b = JB07-90; c = JB07-87A,C; d = TK07-36; e = JB07-84 and 82A; f = TK07-33; 1 = SM-127; 2 = SM-21A; 3 = Q; 4 = SM-172; 5 = SM-92A; 6 = SM-135B (muscovite and K-feldspar); and 7 = HU-2 (muscovite and K-feldspar).

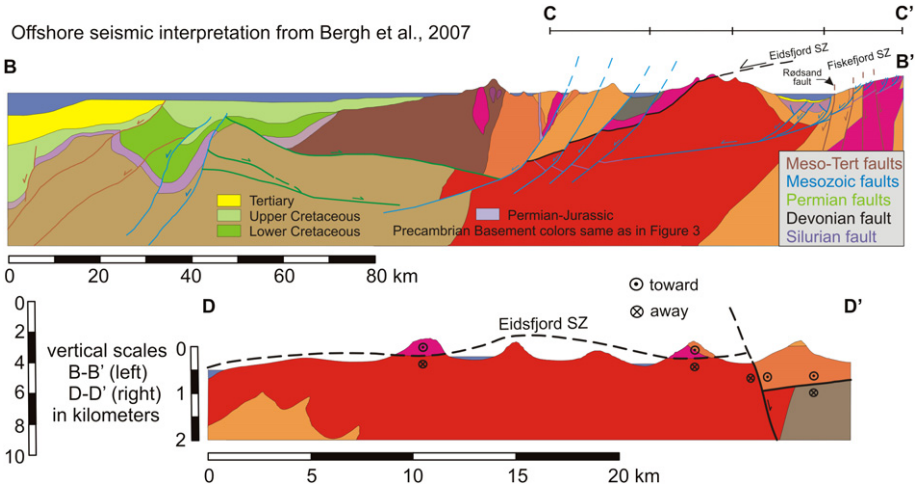

Fig. 4. Geologic cross sections of the Eidsfjord and Fiskefjord shear zones. Lines of sections are depicted in Figs. 2 and 3. Light-brown-colored lowermost unit in the western-half of section B–B′ is unexposed Precambrian basement.

foliation in retrograded monzonite, anorthosite, and mangerite. S_1 mostly dips moderately to the north, with strikes varying from NW to NE (Fig. 6A). S_1 is overprinted by mylonitic deformation associated with the Eidsfjord shear zone (Fig. 5), but outside of about 100 m of the shear zone, S_1 has not been completely obliterated and retains most of its original structures and high-grade mineral assemblages. The S_1 foliation is weakly developed in most areas and generally consists of a compositional banding of feldspar/quartz with biotite and other mafic minerals.

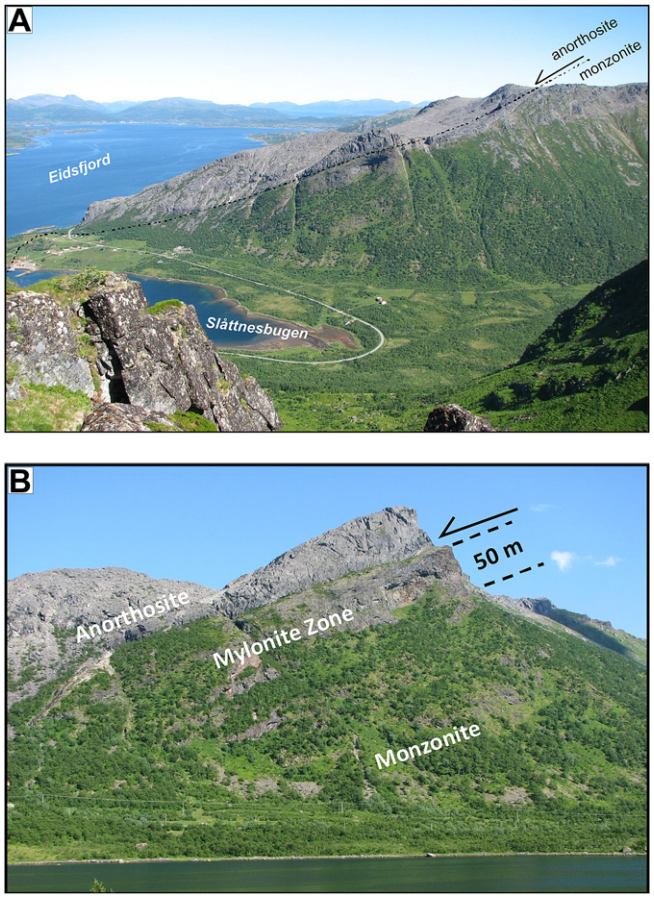

Fig. 5. A. Photograph of the Eidsfjord detachment facing northeast across Slåttnesbugen. B. Photograph facing northeast across Slåttnesbugen illustrating the thickness of the Eidsfjord detachment.

An idealized composite section across the Eidsfjord shear zone is illustrated in Fig. 7. Strike of mylonitic foliation in the shear zone, S_2, is roughly E–W with dip ranging from 7 to 35°NW and the detachment surface dipping ~25° (Figs. 4 and 6B). The footwall is coarse-grained monzonite with minor biotite gneiss and amphibolite. The hanging wall is predominantly massive, coarse-grained, gray anorthosite (plagioclase + orthopyroxene). Mylonites record noncoaxial simple shear strains with abundant shear-sense indicators that consistently record tops-west, normal-slip displacement (Fig. 8). Mylonitic foliation and normal-slip shear bands, S-C fabrics, and asymmetric folds above the main detachment surface develop sharply downward in the meta-anorthosite over a distance of 1–2 m (Fig. 7). Mylonitic foliation is in part compositional, defined by alternating biotite + hornblende and plagioclase-rich layers, and partly by preferred orientation of biotite and hornblende (Fig. 8B). Anastomosing networks of ultramylonite that encapsulate lenses of weakly deformed anorthosite are found directly above the detachment surface (Fig. 9A). Mylonitized monzonite in the footwall contains abundant sigma and delta porphyroclasts, broken-displaced grains, shear bands, and S-C fabrics with tops-west normal-slip shear sense (Fig. 8C and D). Mylonites disappear ~100 m structurally downward into the monzonite by way of anastomosing shears that surround weakly deformed lenses that finally give way to centimeter thick shears along the margins of competent mafic bodies. The detachment surface is abrupt and remarkably planar Fig. 9B. Anorthosite is locally observed in direct contact with monzonite but more commonly a thin (meter scale) zone of densely spaced, domino-style, tops-west, brittle-normal faults mixed with cataclasite, ultracataclasite, and pseudotachylyte mark the detachment (Fig. 9C and D). In most localities steeper brittle faults merge into the detachment, but locally brittle faults cut the detachment surface (Fig. 9B).

Shallow NW-plunging, slip-parallel, folds are observed on both macro- and mesoscopic scales (Figs. 3, 4 and 10). Lower-hemisphere stereographic projections of poles to mylonitic foliation, S_2 (Fig. 6B), have a best-fit great circle with β-axis at N74°W, 9°, which corresponds to the axis of macroscopic antiforms and synforms that fold the Eidsfjord shear zone (Figs. 3 and 4). Elongation lineations, L_2, in the mylonites (Fig. 6C) are mostly shallow plunging and dispersed around an east–west axis, coaxial with axes measured for mesoscopic sheath folds (Fig. 10); the slipline, N72°W,

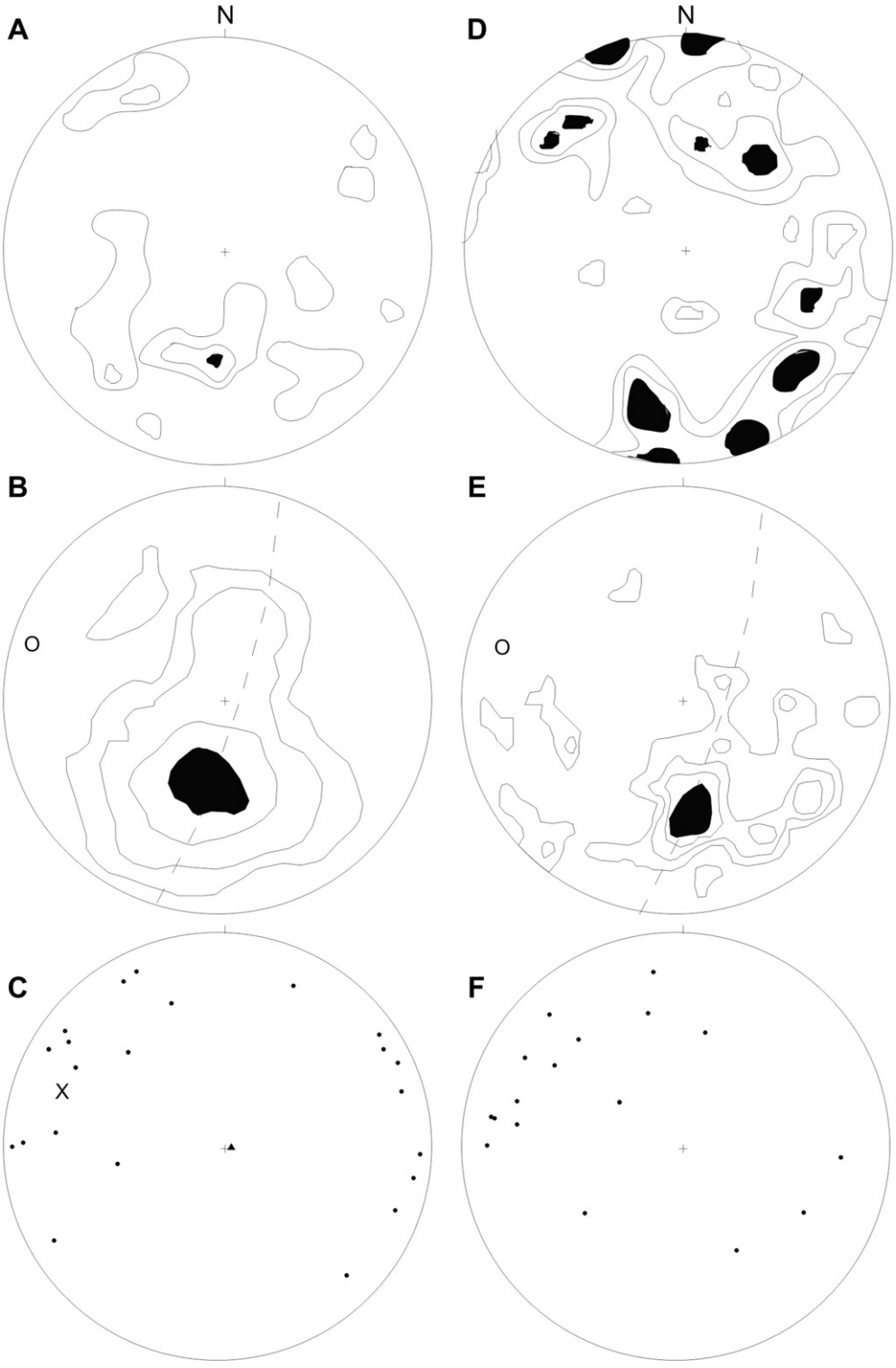

Fig. 6. Equal-area, lower-hemisphere stereographic projections of Eidsfjord (left column) and Fiskefjord (right) structures. A and D: contoured poles to S_1; $n = 58$ and 135, respectively; contour interval (CI) = 1% per 1% area. B and E. Contoured poles to S_2, visual best-fit great circle with β-axis (O) at N74°W, 9°; $n = 104$ and 47, respectively; CI = 2% per 1% area. C and F: Elongation lineations, L_2, in mylonite; $n = 24$ and 17, respectively; X = best-fit slipline (see text).

25°, corresponds to the down-dip point concentration of L_2 measurements. Sheath fold axes trend shallowly NW–SE parallel to transport and where they make a high angle to the direction of slip they are consistently asymmetric and west-vergent (Fig. 10), corroborating tops-NW (extensional). Coaxiality between the determined slipline and the axis to the macroscopic folds implies that they are corrugations formed during transport along the Eidsfjord detachment, similar to those reported for the Nordfjord–Sogn detachment in west Norway (Osmundsen and Andersen, 1994; Osmundsen et al., 1998, 2003).

Syn- and/or post-detachment faulting have excised the Eidsfjord detachment to the northeast (Fig. 1) and its trace beneath the

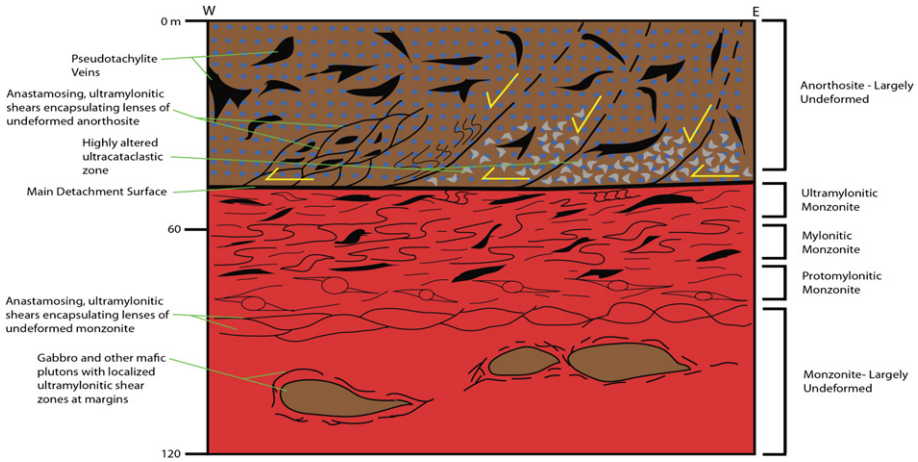

Fig. 7. Idealized section illustrating pseudotachylyte distribution and deformational structures of the hanging wall anorthosite and the footwall monzonite across the Eidsfjord detachment.

surface of Eidsfjord to the southwest also is undetermined. Parallelism between the axial traces of the macroscopic corrugation folds with the trace the high-angle left-slip fault that has excised the Eidsfjord detachment leads us to interpret the latter structure as a transfer fault similar to those that segment the Nordfjord–Sogn detachment (Osmundsen and Andersen, 1994; Osmundsen et al., 1998, 2003). Understanding the geometries of the corrugations and the transfer faults helps to explain why the Eidsfjord detachment is isolated within synformal 'tucks' exposed along Eidsfjord (Fig. 3).

Tveten (1978) indicated another shear zone to the east of Eidsfjord in the Fiskefjord area. Løseth and Tveten (1996) later reported these to be short isolated segments of shallow-dipping shear zones associated with pseudotachylite that are cut by later, higher-angle brittle faults. No detailed structural observations or absolute timing constraints were reported, however, leading us to initiate geometric, kinematic, rheological, and $^{40}Ar/^{39}Ar$ isotopic investigations on the shear zones and brittle faults. In addition to being less continuous in strike length than we had expected, we found the Fiskefjord shear zones to occur at seemingly random structural levels (Mager, 2005). The longest, most continuous exposure (~600 m) of a through-going plastic shear zone is exceptionally well exposed in a south-facing cliff directly north of Fiskjordvatnet (Figs. 3 and 11). Here, several moderate-to-steep dipping, narrow (<5 m thick; Fig. 11A and D), tops-west brittle-ductile splays shallow with depth and merge with and reactivate the main, relatively high-temperature shear zone (Fig. 4, cross section C–C′). This main shear zone was the structurally lowest one

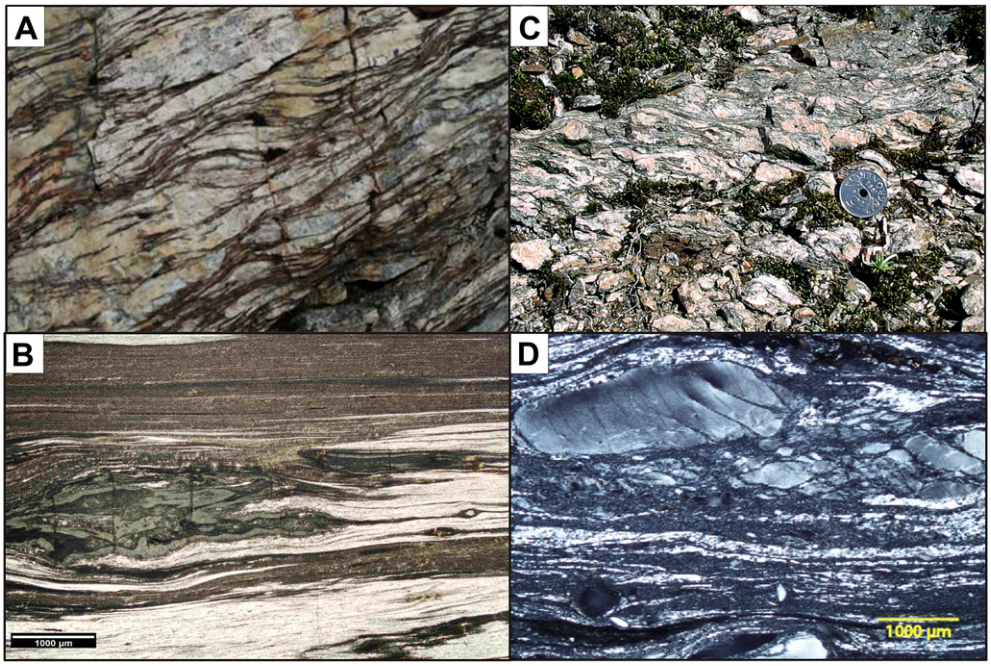

Fig. 8. A. Tops-down-to-the-west (left) S-C fabrics in mylonitized anorthosite from directly above the Eidsfjord detachment surface. Long dimension of the photograph is 14 cm. B. Photomicrograph (ordinary light) of alternating bands of dynamically recrystallized quartzofeldspathic and amphibole-biotite aggregate in upper plate anorthosite ultramylonite (PPL). C. Tops-west normal-slip S-C fabrics in mylonitized monzonite from the Eidsfjord detachment lower plate. D. Photomicrograph (PPL) of partially broken and displaced (tops-left/west) K-feldspar porphyroclasts in mylonitized monzonite of the lower plate.

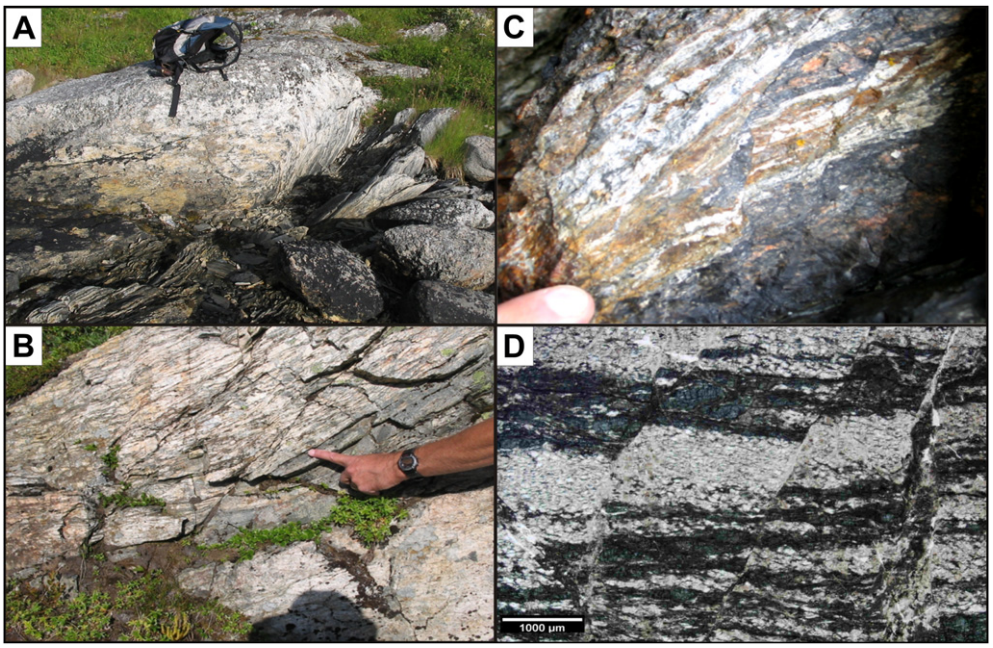

Fig. 9. Features associated with the Eidsfjord detachment. A. Weakly deformed lense of anorthosite encapsulated by thin, ultramylonitic shears directly above the detachment surface. B. Moderately west (left)-dipping normal faults cross-cutting anorthosite ultramylonite and the main Eidsfjord detachment surface. Finger points to detachment surface. C. Tops-west (left) normal faults cutting ultramylonite and pseudotachylite in hanging wall directly above detachment surface at Slåttnesbugen. D. Photomicrograph (ordinary light) of tops-west brittle faults displacing ultramylonitic banding in anorthosite at Grønning.

that we observed, and we call it the Fiskefjord shear zone. Earlier-formed tops-east thrust indicators within mylonites of the Fiskefjord shear zone have been reactivated by tops-west mylonitic shears (Fig. 11C). We interpret the other structurally higher segments of tectonite, mylonite, ultramylonite, and pseudotachylyte developed within mangerite, granitic gneisses, and biotite amphibolites to be splays within the upper plate of the Fiskefjord shear zone (Fig. 4).

Like the Eidsfjord shear zone, the Fiskefjord shear zone does not appear to have disturbed the S_1 foliation more than 100 m away from it. Mylonitic foliation, S_2, defining the Fiskefjord and its associated shear zones generally parallels that of the Eidsfjord shear zone (cf., Fig. 6B and E). S_2 appears to be weakly folded about precisely the same β-axis as determined for the Eidsfjord shear zone; a weak partial girdle of S_1 folia mimics that of the S_2 partial girdle, likely reflecting deflection of S_1 into the shear zones proximal to their margins. Most of the northeast-striking shear zones have shallower dips and down-dip slip lines (Fig. 6F) with normal, tops-west, dip-slip movement, also mimicking the Eidsfjord shear zone. A number of the northwest-striking shear zones in the

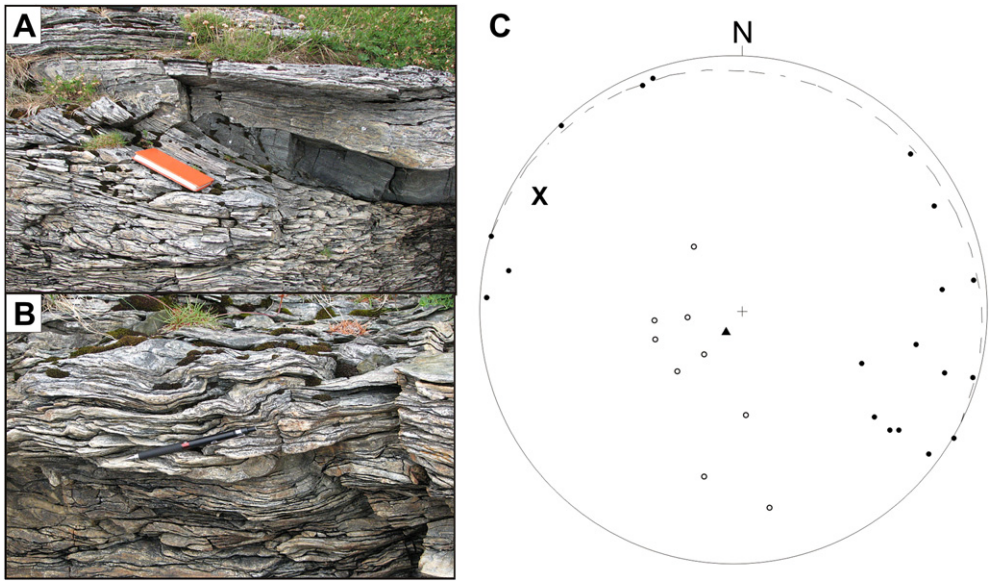

Fig. 10. A. and B. Tops-west (left in photos) intrafolial folds of ultramylonitic banding in anorthosite. C. Sheath fold axes (dots) dispersed within visual best-fit great circle (dashed) and its pole (triangle); open dots are poles to axial surfaces of the sheath folds. Large X is a pronounced NW-trending 'tube' axis measured in outcrop. Sheath axes trend shallowly NW–SE parallel to transport, whereas asymmetric folds at high angles to the sheaths are wholly NW vergent, documenting tops-down-NW (extensional) movement.

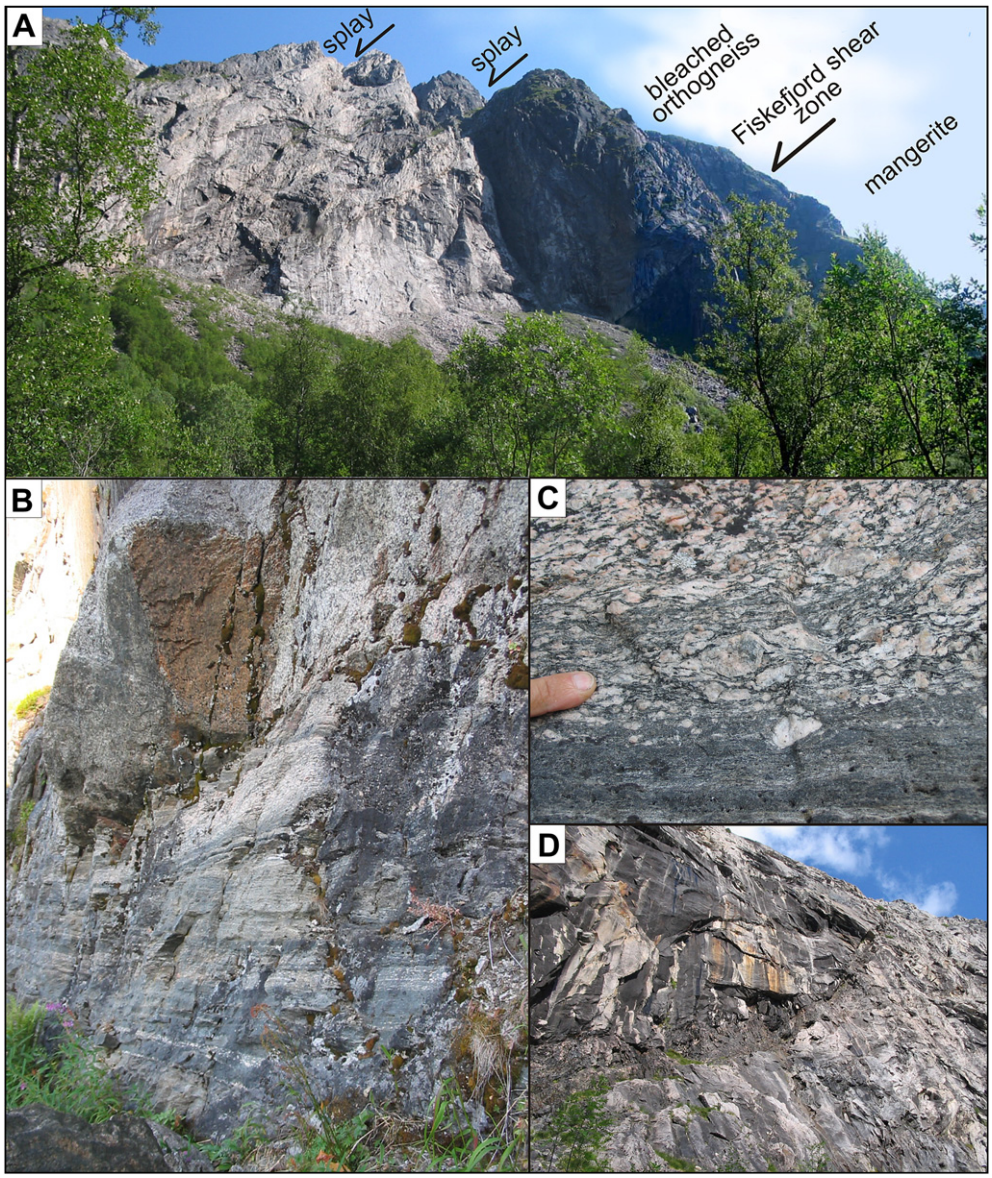

Fig. 11. Fiskfjord shear zone with several later-formed splays. A. View looking northeast from Fiskjordvatnet (Fig. 3). B. Exposed section across the high-temperature Fiskfjord shear zone (center, dipping slightly toward the left [west]) with massive orthogneiss (light colored) above becoming progressively mylonitized structurally downward into mylonitized monzonite (darker and layered). C. Close up view of tops-down-to-the-west (left in photo) S-C fabrics and K-feldspar sigma clasts in layered monzonitic orthomylonite (upper) and ultramylonite (lower) of the lower plate. Finger tip at left for scale. D. Listric, brittle-ductile splay (westernmost one in Fig. 11A) that roots into and has reactivated the high-temperature Fiskfjord shear zone. (For interpretation of the references to colour in this figure legend, the reader is referred to the web version of this article.)

Fiskefjord area have relatively steeper dips with elongation lineations that are sub-parallel to strike, indicating oblique, strike-slip movement (Mager, 2005).Quite a few of the Fiskefjord shear zones coincide with the locations indicated by Løseth and Tveten's (1996; their 'inferred faults'). Brittle fractures and faults that we measured in the study area (Fig. 12A) coincide geographically with faults reported by Løseth and Tveten (1996) and support their suggestion for principally two trends of predominantly steep-dipping brittle faults, one NNE- and one WWE-trending.

3. Mineralogy and petrology of fault rocks

A variety of fault rock types within the Eidsfjord and Fiskefjord areas, ranging from high-temperature mylonites to cataclasites to pseudotachylytes (Figs. 7 and 9), contain microstructures and assemblages clearly documenting that they have retrograded the earlier-formed granulite- and amphibolite-facies assemblages of the meta-igneous protoliths. Amphibolite-facies retrogression converted granulite-facies assemblages into cpx + hbl + plg + bt + qtz and hbl + bt + plg + qtz assemblages. The highest temperature mylonites have cpx porphyroclasts deformed by dislocation glide indicating temperatures of deformation between 500 and 700 °C (Buatier et al., 1991), compatible with amphibolite-facies metamorphism that caused the partial to complete retrogradation of cpx to hbl in proto- to ultramylonites (Fig. 8B). Amphibole forms sigma-type porphyroclasts but less is known about the temperature regime of plastic deformation of amphibole beyond that they are stronger than pyroxenes (Passchier and Trouw, 1996). Porphyroclastic garnet is common in most ultramylonite samples but they are not drastically rounded or fractured. Intracrystalline feldspar microstructures in the higher temperature mylonites include core-mantle structures, deformation lamellae, undulose extinction, microkinks, and myrmekite development (Fig. 8D). Feldspar recrystallization and the growth of strain-related myrmekite are consistent with

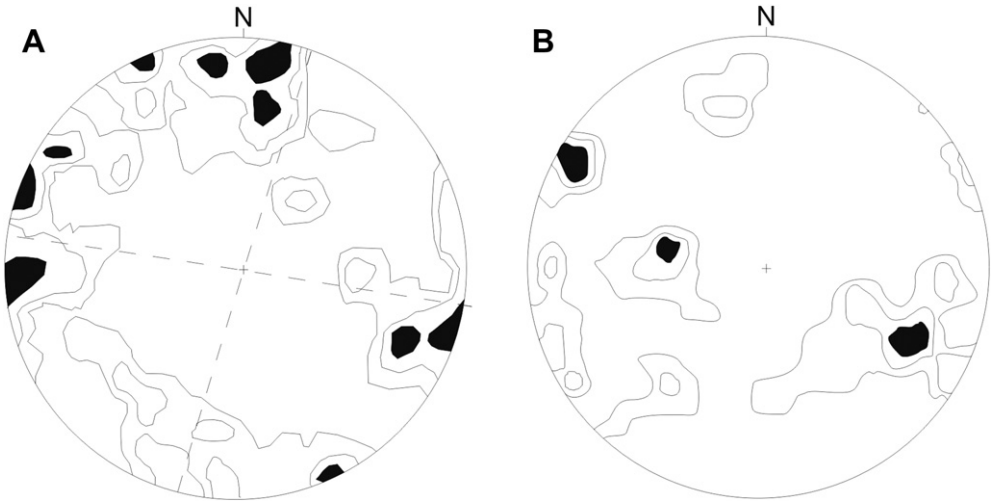

Fig. 12. Contoured, equal-area, lower-hemisphere stereographic projections of poles to post-S_2 mylonitic structures in the Fiskefjord area. A. Brittle fractures and faults: $n = 107$; contour interval (CI) = 1% per 1% area. Dashed great circles correspond to two principal fracture/fault sets based on point maxima concentrations. B. Pseudotachylytes: $n = 38$; CI = 2% per 1% area.

temperatures >500 °C (Passchier and Trouw, 1996). Lower temperature mylonites contain crystal-plastic quartz together with brittle, microfaulted feldspar, bracketing their deformational temperatures to between ~450 and 300 °C (Voll, 1976; Tullis, 1983). Cataclasites contain clasts derived from all of the above mentioned protoliths and mylonites (Fig. 9C and D) and document exhumationof the Eidsfjord shear zone above the brittle-ductile transition.

Pseudotachylyte veins associated with the Eidsfjord shear zone are developed in granulite-facies anorthosite and migmatitic gneiss of the hanging wall, decreasing in abundance upward from the detachment (Plattner et al., 2003). Hanging wall occurrences are fracture, reservoir and pseudobreccias types characteristic of brittle pseudotachylyte (Sibson, 1975; Plattner et al., 2003). Hanging wall pseudotachylite contains abundant evidence of a melt origin, including glass, variably molten and flattened feldspar clasts, and quench crystals of feldspar.Meta-anorthosite at the base of the hanging wall in the Eidsfjord shear zone becomes bleached white and variably recrystallized (porphyroclastic protomylonite to ultramylonite) to a lower amphibolite-facies assemblage of plagioclase + hornblende + biotite + ilmenite ± muscovite + epidote ± scapolite ± titanite ± garnet (Moecher and Steltenpohl, 2009, 2011). Pseudotachylyte occurs at the base of the anorthosite that is progressively bleached approaching the detachment. Altered pseudotachylyte veins and relict clasts are apparent in the mylonitic bleached meta-anorthosite.

Within the Eidsfjord ductile detachment zone, pseudotachylyte fills fractures parallel to and cross-cutting the foliation in mylonitic meta-anorthosite and monzonitic gneiss formed during normal coaxial deformation. Mylonitized pseudotachylyte and folded pseudotachylyte veins are also common within the detachment. Several generations of pseudotachylite, folded and metamorphosed pseudotachylite, and the thickest and greatest concentration of pseudotachylite are present in the most strongly deformed rocks at the top of the detachment at Grønning where breccias consist of clasts of mylonitic meta-anorthosite in pseudotachylite. The extremely fine-grained mylonites with dynamically recrystallized plagioclase contain tiny syntectonic garnets (Moecher and Steltenpohl, 2009, 2011).

Mineral assemblages and fabrics in the Fiskefjord shear zone suggest a higher temperature extensional deformation history at deeper crustal levels. Mylonitic gneisses and tectonites preserve variably recrystallized garnet and clinopyroxene. Pseudotachylites generally are <1 cm thick, though some are up to 14 cm thick (Mager, 2005). They are mostly planar and tabular, striking ~ N27°E and dipping steeply to moderately toward the east and west (Fig. 12B), and have numerous wispy branches or wedges shooting off from the reservoir vein. Pseudotachlyte veins in granulite-facies mangerite of the Fiskefjord shear zone are cut by normal-sense (tops-NW) shear bands that produce mylonitic to ultramylonitic pseudotachylyte striking N20°E and dipping 60° NW, with an oblique lineation defined by feldspar and pseudotachylite streaks oriented N42°E to N20°W. Recrystallized clinopyroxene and plagioclase clasts in ultramylonitic have reacted to form garnet. The undeformed pseudotachylyte veins have recrystallized statically to garnet + hornblende-bearing assemblages. Pressure and temperature conditions for the ductile recrystallization event in the Fiskefjord shear zone, calculated from garnet-clinopyroxene-plagioclase-quartz geobarometers and geothermometers, are 950 ± 150 MPa at 625–675 °C (Moecher and Steltenpohl, 2009, 2011). The calculated pressure interval corresponds to a depth interval of 35 ± 5 km.

4. $^{40}Ar/^{39}Ar$ thermochronology

As already mentioned, the paucity of Caledonian metamorphic and deformational relics in the Lofoten–Vesterålen basement is a long-standing problem. Part of the problem stems from the fact that this metaplutonic basement complex is largely granitic in composition, and though granite-on-granite shears are common, they might have formed at literally anytime since the Archaean.Workers have found that documenting the Caledonian structures requires tediously detailed field and structural investigations in combination with targeted isotopic age dating (Tull, 1978; Griffin et al., 1978; Bartley, 1982; Coker et al., 1995; Hames and Andresen, 1996; Plattner et al., 2003; Steltenpohl et al., 2003a, 2004; Corfu, 2004). Given that the study area is positioned between the Caledonian nappe stack to the east and the suspect Lofoten terrane basement to the west (Fig. 2), our principle aim is to characterize the timing of movement along the retrograde mylonites and pseudotachylites found in exceptional abundance in the study area. $^{40}Ar/^{39}Ar$ analyses were performed on muscovite, biotite, and potassium feldspar grains that were sampled and analyzed using two different laboratories to address three separate timing issues. The single-crystal fusion $^{40}Ar/^{39}Ar$ analyses on muscovite were performed in the Auburn

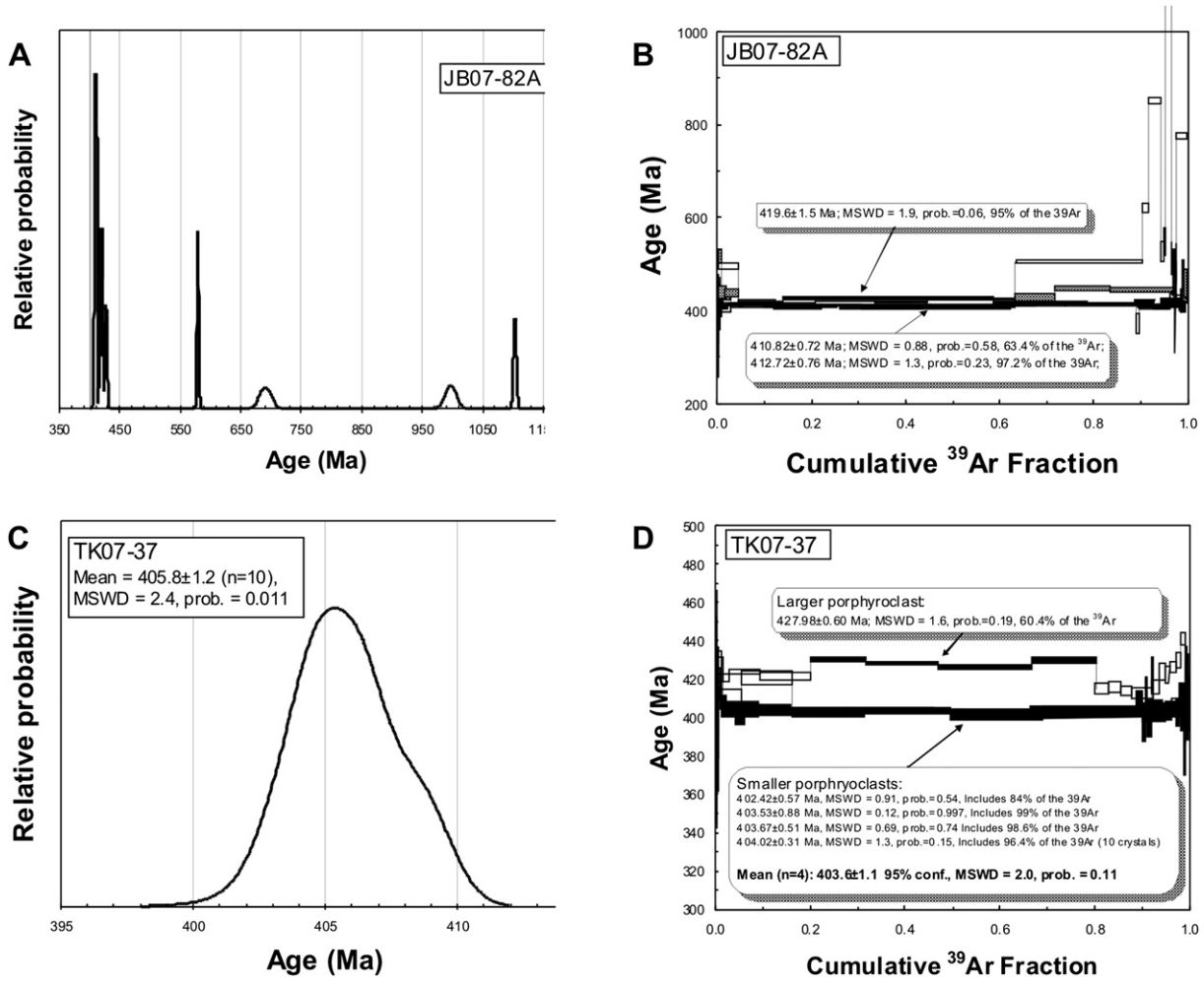

Fig. 13. Data representing laser $^{40}Ar/^{39}Ar$ analyses for muscovite from six samples in the poresent study (see appendix for complete data set). A. Probability distribution for single-crystal total fusion ages for muscovite from sample JB07-82A; B. Five incremental heating spectra for single muscovite crystals from sample JB07-82A. C. Probability distribution for single-crystal total fusion ages for muscovite from sample TK07-37; D. Five Incremental heating spectra from sample JB07-82A, four from single muscovite crystals and one from a multigrain sample of ten crystals.

Noble Isotope Mass Analytical Laboratory (ANIMAL)[1] to constrain the timing of movement along the Eidsfjord shear zone. $^{40}Ar/^{39}Ar$ step-heating isotopic analyses on muscovite and K-feldspar were done in the U.S. Geological Survey geochronologic facility in Denver, Colorado, under the direction of Mr. M. Kunk. The step-heating analyses were aimed at exploring the pre-detachment history of rocks forming the upper plate, and also to deduce the time of movement along several brittle faults that either cut or merge with the detachment fault (see Appendix 1 for methods). The sample locations are illustrated on Fig. 3. The samples and their respective $^{40}Ar/^{39}Ar$ analytical results are reported in Appendix 2 and described below. Although dependent on cooling rate and mineral composition, most workers agree that the closure temperature ranges for muscovite and K-feldspar are 350–400 °C and 150–250 °C, respectively (see McDougall and Harrison, 1999). These closure temperature ranges will be used in the interpretations and discussions below.

4.1. Eidsfjord shear zone

$^{40}Ar/^{39}Ar$ single-crystal fusion analyses for fabric-forming muscovite were performed on six samples collected from ultramylonitic anorthosite along the base of the upper plate to the Eidsfjord detachment (Fig. 3). Our analytical strategy was chosen to efficiently resolve differences in age for recrystallized, neoblastic and relict, porphyroclastic muscovite: ten crystals were selected from each sample for single crystal total fusion, and then additional crystals were chosen from the samples with the lowest and highest variance in fusion ages for single-crystal incremental heating analyses. Results from this approach are represented in Fig. 13.

The single-crystal fusion analyses resulted in modes of ca. 405 Ma for each sample, however some samples, such as JB07-82A (Fig. 13A), yielded muscovite crystals with ages up to ca. 1075 Ma. Five single-crystal incremental heating spectra obtained for sample JB07-82A are highly variable in character. Plateau ages of 410.8 ± 1.4 and 412.7 ± 1.5 Ma are defined for two crystals from JB07-82A (each with ~95% of the $^{39}Ar_K$ released, all ages quoted at 2σ, see Fig. 13B); however, three other crystals from this sample yield discordant spectra with ages up to ca. 1000 Ma in higher temperature release steps. This pattern of age discordance is indicative of relict ^{40}Ar inherited from muscovite that formed in pre-Caledonian event(s), and not extraneous 'excess' argon in defects, and therefore the older ages provide minimum constraints to the age of the original muscovite. We interpret the results for JB07-82A to reflect partial recrystallization of Proterozoic muscovite with an age of ca. 1.1 Ga or older during Caledonain event(s).

[1] Data Repository item.

All of the single-crystal fusion ages for muscovite from sample TK07-37 are ca. 405 Ma (Fig. 13C), with a mean of 405.8 ± 1.2 Ma, though a relatively high variance for the ages (MSWD = 2.4) indicates some scatter beyond the precision of measurement. All of the incremental heating analyses from this sample yielded plateau ages (Fig. 13D). A single, notably larger porphyroclast from the sample (ca. 2 mm in diameter) yielded a somewhat variable spectrum of ages and defined a plateau age of 419.6 ± 3.0 Ma (MSWD = 1.9, prob. = 6%, 95% of the $^{39}Ar_K$ released). Three other smaller single crystals (about 1 mm in diameter) yielded plateau ages of 402.4 ± 1.1, 403.5 ± 1.8, and 403.7 ± 1.0 Ma (each with MSWD less than 1 and comprising more than 80% of the $^{39}Ar_K$ released). In view of these results, we selected ten small, equant crystals (~0.8 mm in diameter) from this sample for a combined incremental heating experiment, and obtained a plateau age of 404.02 ± 0.62 Ma (MSWD = 1.3, with 96% of the $^{39}Ar_K$ released). Considering the consistency of single-crystal fusion and incremental heating ages for non-porphyroclastic muscovite from TK07-37, and the sample context, we interpret the ages obtained to reflect the timing of crystallization for the muscovite during the main fabric-forming deformation event in the Eidsfjord detachment. Combining our incremental heating results for sample TK07-37, we suggest the mean age of 403.6 ± 1.1 Ma (MSWD = 2.0, prob. = 11%) is the best estimate for the timing of this event.

Early Devonian movement along the Eidsfjord shear zone is compatible with it having retrograded metamorphic assemblages formed during the peak of the Scandian collision (429–432 Ma) as documented in basement and allochthonous cover rocks throughout the Ofoten region (Coker et al., 1995; Northrup, 1997; Steltenpohl et al., 2003b, 2009). Our ~404 Ma age for tops-west movement is identical to $^{40}Ar/^{39}Ar$ muscovite ages reported from the same structural position along the Nordfjord–Sogn detachment (Berry et al., 1995; Andersen et al., 1998; Hacker et al., 2006). Also like the Nordfjord–Sogn, muscovite cooling dates previously obtained for the region progressively decrease structurally downward into the Eidfjord's lower plate, but they reach much younger ages than are reported from the former detachment (Permian rather than Late Devonian: Hames and Andresen, 1996; Steltenpohl et al., 2004; Key et al., 2008). Our muscovite dates also are compatible with an attempt by Plattner et al. (2003) to date pseudotachylite from the Eidsfjord area using $^{40}Ar/^{39}Ar$ methods that suggested a Devonian to Carboniferous age.

4.2. Fiskefjord shear zones

Seven rock samples were selected from the Fiskefjord area from which muscovite, biotite, and K-feldspar were analyzed using $^{40}Ar/^{39}Ar$ step-heating isotopic methods (see Steltenpohl et al., 2009, for methodology and references). All of these samples were from shear zones or faults or from their shoulder/country rocks from different parts of the study area (Fig. 3). Most of the muscovite profiles are complex, with only one (HU-2) yielding a plateau age (Fleck et al., 1977: Fig. 14). Attempts using $^{36}Ar/^{40}Ar$ versus $^{40}Ar/^{39}Ar$ inverse-isochron correlation plots did not reveal meaningful ages for any of the complex spectral analyses. Three biotite concentrates were analyzed by fusion analysis but they yielded ages older than muscovite dated from the same specimen, implying geologically meaningless ages likely due to incorporation of extraneous ^{40}Ar.

Sample SM-21A (#2 in Fig. 3) is from migmatitic gneiss collected less than a meter from a northwest-striking shear zone. The muscovite grains ranged in size from 0.02 to 0.025 mm and form the gneissic foliation rather than a deformed remnant of that fabric. The spectrum for SM-21A (Fig. 14) has a hump throughout the first half of the heating steps, climbing to ~590 Ma and then descending to a ~550 Ma saddle before gradually stepping back up to 590 Ma. There is a sympathetic relationship between K/Ca and heating-step age, which may indicate compositional control, perhaps by tiny inclusions within the grains. The saddle age of ~550 Ma likely represents a maximum age for the sample, but little more can be gleaned from the analysis.

Muscovite sample SM-172 (#4 in Fig. 3) was taken from a migmatitic gneiss less than a meter from a northeast-striking shear zone associated with the Fiskfjord shear zone. Muscovite from this sample ranges from 0.07 to 0.43 mm in length and forms the schistosity. The smaller grains commonly are 'peels' that have phacoidal shapes and are clearly derived through post- crystallization shearing of the larger grains. The age-release spectrum for SM-172 has a similar architecture (i.e. a single-hump) and slightly younger age range (~501–561 Ma) to that of SM-21A (Fig. 14), and the ~514 Ma saddle is a maximum age for the sample.

Sample SM-135B (#6 in Fig. 3) is from a migmatitic gneiss collected from near a northwest-striking shear zone. This shear zone is associated with the northwest-striking Djupfjord fault (Fig. 3). Muscovite ranges from 0.1 to 1.0 mm in length and helps to define the gneissosity, but thin peels and fish are clearly derived from larger muscovites from the shoulder rocks to the shear zone. The age-release profile is relatively flat but did not plateau (Fig. 14).

Muscovite sample SM-127 (#1 in Fig. 3) is from a schistosity-forming population separated from a schist sample collected from the migmatitic gneiss complex located near a minor, localized, northeast-striking shear zone; there was no microstructural indication, however, to suggest that the muscovite experienced any strain related to this zone. Muscovite is idioblastic and ranges from 0.2 to 0.75 mm in length. The age spectrum for SM-127 has two humps, both with maximum ages at ~580 Ma (Fig. 14).

Sample SM-92A (#5 in Fig. 3) was taken from a feldspathic schist of the migmatitic gneiss complex less than a meter from a northeast-striking shear zone located just east of Djupfjord (Fig. 3). It contains sparse, fine-grained 0.03 mm muscovite. Again, the age spectrum (Fig. 14) has a weak, single-hump architecture, with ages ranging from 434 to 454 Ma (disregarding the first two and last steps, which together account for only 1% ^{39}Ar with relatively lower radiogenic yields); the total gas age is 438 Ma.

Sample HU-2 (#2 in Fig. 3) was collected less than a meter from the shear zone exposed at Husvik. This migmatitic rock has biotite-feldspar schist melanosomes mixed with muscovite-biotite pegmatitic leucosomes. Muscovite from the leucosomes are up to 1 cm in length, are not deformed, and define the schistosity. The 456.9 ± 2 Ma age is the only plateau age recorded by any of the analyzed specimens (Fig. 14).

Samples SM-135 and HU-2 (#s 6 and 7, respectively, in Fig. 3) also contained potassium feldspar that was separated and analyzed for $^{40}Ar/^{39}Ar$ isotopes (Fig. 14). Potassium feldspar from SM-135B was up to 0.75 mm in length and flattened parallel to the gneissosity. Potassium feldspar from HU-2 was up to 4 mm in length and contained numerous sericite inclusions and tartan twin planes. Both analyses resulted in similar diffusional-release profiles. The diffusional gradient for SM-135B has a maximum age step of ~460 Ma and a minimum at ~235 Ma; Hu-2 was ~438 and ~185 Ma, respectively.

Sample Q was taken from the quarry at Rødsand (#3 in Fig. 3) within a major fault that cuts the gneiss complex; we interpret this fault to be an exposed segment of a fault related to the Hadslefjord fault zone (Hendriks et al., 2010).Breccias and gouge from the Rødsand fault were noted to locally overprint higher temperature brittle-ductile transitional mylonites (Mager, 2005). Potassium feldspar from the sample we analyzed was up to 1 cm in diameter, broken and veined, and salmon-pink colored, the result of flushing of the zone by hot hydrothermal fluids during faulting. This

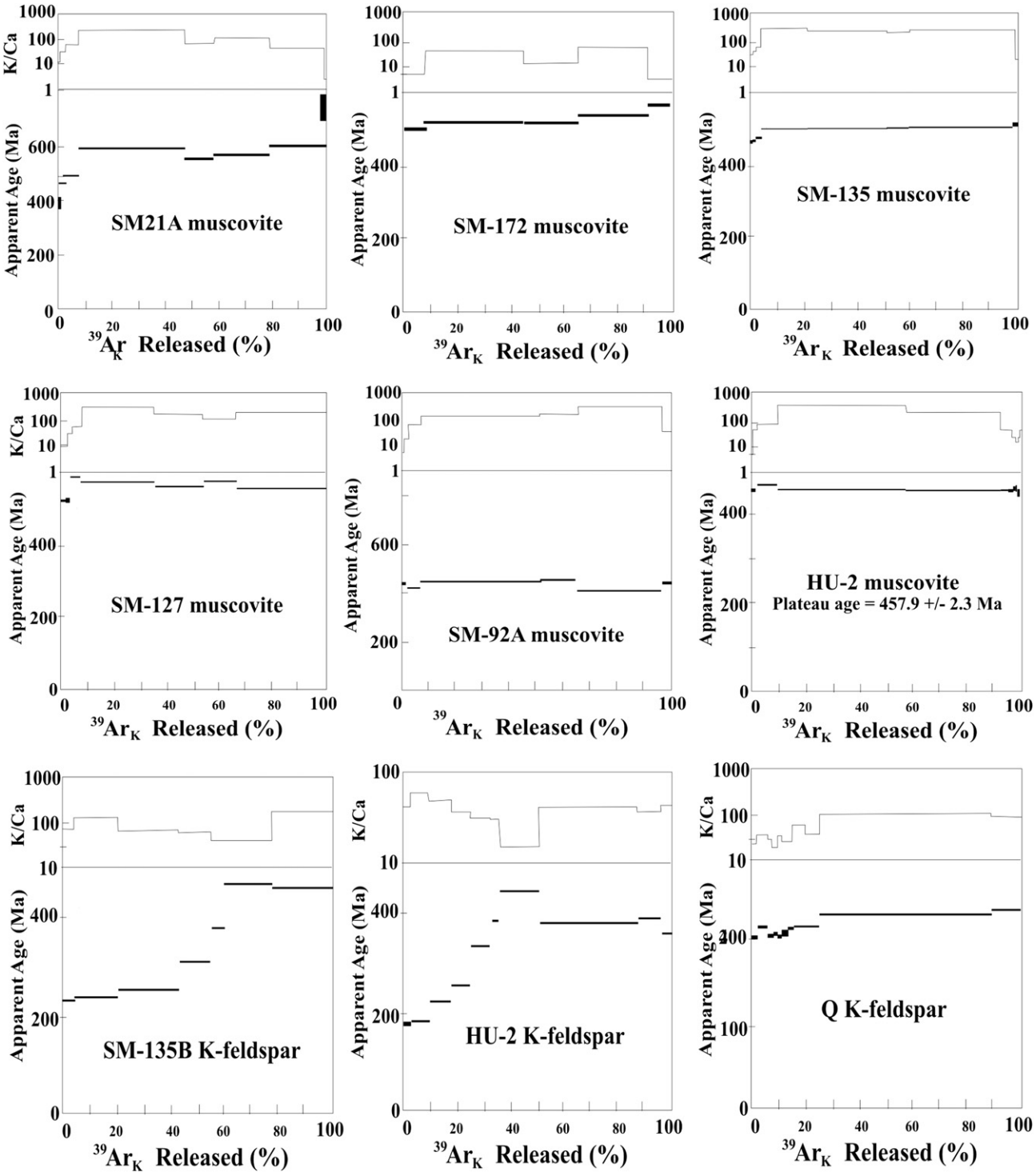

Fig. 14. $^{40}Ar^{39}Ar$ step-heating analyses of muscovite and K-feldspar samples from the Fiskefjord area.

diffusional-release profile has a much more condensed distribution of heating-step dates than in the other K-feldspar analyses, ranging from 239 Ma to ~207 Ma (Fig. 14).

We interpret the muscovite $^{40}Ar/^{39}Ar$ step-heating spectra from the Fiskefjord area to reflect thermal disturbances that only partially rejuvenated older extraneous components from the original Precambrian metamorphic minerals within the upper plate to the Fiskefjord extensional shear zone. The best control on the time of cooling through the ~350 °C isotherm is the 457 Ma plateau date of Hu-2. This date requires that the upper plate to the Fiskefjord shear zone maintained high-crustal levels throughout the Scandian event, and it presents a distinct older-age anomaly in the westward-younging pattern of $^{40}Ar/^{39}Ar$ muscovite ages reported earlier for Lofoten–Vesterålen (Coker et al., 1995; Steltenpohl et al., 2004). Middle-Ordovician cooling of upper-plate rocks is compatible, however, with recently reported U–Pb dates for eclogite-facies metamorphism of rocks on Flakstadøy at ~478 Ma (Steltenpohl et al., 2010b, 2011) and subsequent amphibolite-facies

metamorphism of the Leknes Group between 461 and 469 Ma (Corfu, 2004). It is becoming more apparent that Lofoten contains an obscure record of Middle-Ordovician tectonothermal activity that needs to be further investigated and compared with that documented for the Seve, Tromsø, and Helgeland Nappe complexes on the mainland, as well as for the Taconic allochthons of the Appalachians on the conjugate side of the collisional belt in North America (Stephens et al., 1993; Roberts, 2003; Steltenpohl et al., 2003a, 2003b, 2011). In contrast to the Eidsfjord shear zone, we find little vestige of Scandian relics associated with the Fiskefjord shear zone. Though our understanding of the kinematics and absolute timing of the Fiskefjord shear zone is relatively limited, the rheology and kinematics of the tops-west mylonitic shears that locally overprint the predominant, earlier-formed tops-east shear zone (Fig. 11C) resemble those that we have described for the Devonian Eidsfjord shear zone. Combined with the common and unique association with pseudotachylites seemingly requires that the tops-west component of both shear zones is the result of Devonian extension.

The potassium feldspar results document Mesozoic pulses of uplift and cooling between ca. 235 Ma and 185 Ma, consistent with Triassic–Jurassic sedimentary basins flanking various parts of the Lofoten Ridge (Dalland, 1975; Brekke and Riis, 1987; Løseth and Tveten, 1996; Mjelde et al., 1996; Davidsen et al., 2001a, 2001b) and with regional $^{40}Ar/^{39}Ar$ mineral cooling patterns (Steltenpohl et al., 2004, 2009).

5. Discussion

5.1. Evolution of the Eidsfjord–Fiskefjord shear zones

Fig. 15 provides a series of cartoon diagrams illustrating our interpretation for the evolution of the Eidsfjord and Fiskefjord shear zones. Basal Caledonian thrusts formed first in an area toward the east of Fiskefjord, and they clearly provided anisotropies that later influenced extensional fault and shear zone geometries and movement histories (Fig. 2). These Caledonian thrusts imbicated thick slices of basement, some several kilometers thick, together with cover units, but in the present study area only basement-on-basement shear zones are present (Hodges et al., 1982; Bartley, 1984; Björklund, 1987; Rykkelid, 1992; Key, 2010). An Early Devonian core complex is hypothesized to have formed between the Of oten synform and Fiskefjord where the basement duplex achieved its greatest structural thickness during the Scandian (Silurian) metamorphic peak (Coker et al., 1995; Northrup, 1997; Steltenpohl et al., 2003b). Uplift of this metamorphic core in the Early Devonian is interpreted to have provided impetus to initiate tops-west motion along the Fiskefjord and Eidsfjord shear zones; 'backsliding' along basal Caledonian thrusts due to far-field effects (Fossen, 1992, 2010; Rykkelid, 1992; Fossen and Rykkelid, 1992; Rykkelid and Andresen, 1994) is not precluded by our observations, but we favor the former interpretation in light of emerging thermochronological evidence from that area (Key, 2010; Steltenpohl et al.,

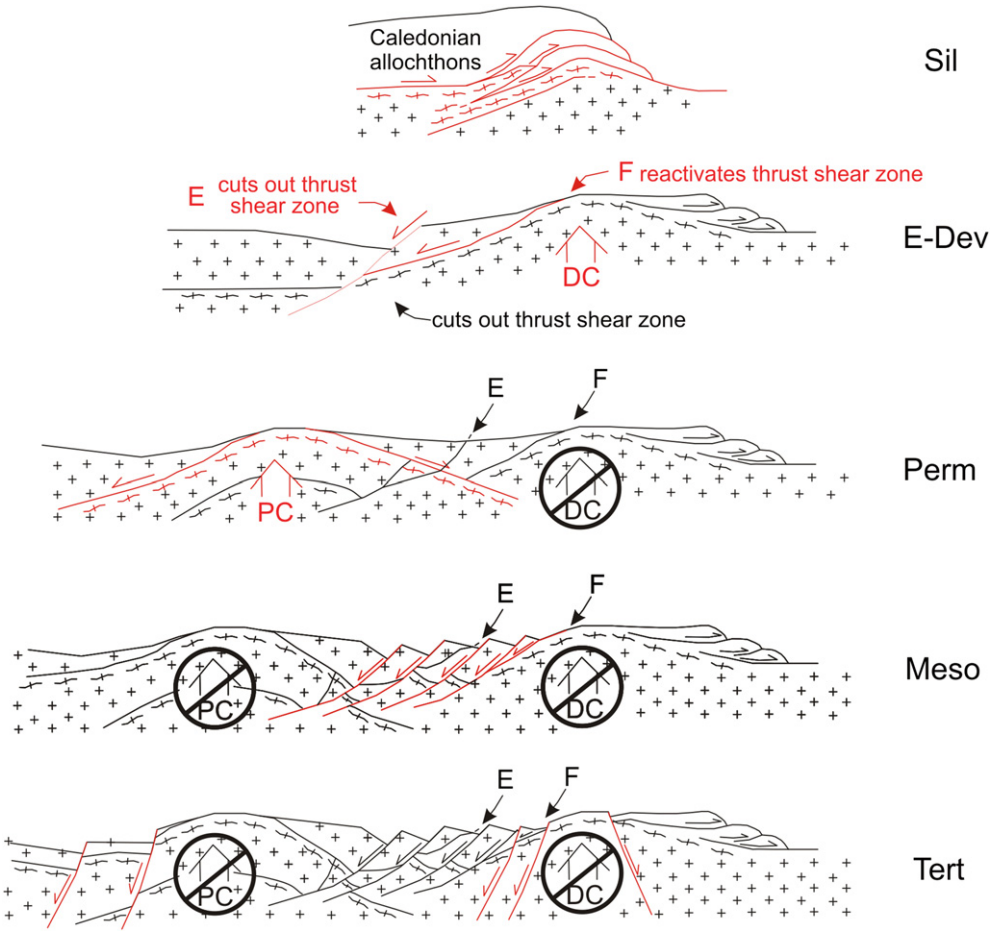

Fig. 15. Series of time-slice cartoon sections (west is to the left) illustrating the evolution of the Eidsfjord (E) and Fiskefjord (F) shear zones. Red features in each section are those that were active during that period of time. Upward pointing arrows illustrate the uplift of Devonian (DC) and Permian (PC) core complexes that later were abandoned (circles with slashes). See text. (For interpretation of the references to colour in this figure legend, the reader is referred to the web version of this article.)

2010b; Anderson et al., 2010). Tops-west normal motion locally reactivated one of the tops-east thrusts forming the Fiskefjord shear zone. The Fiskefjord shear zone apparently was abandoned when tops-west movement was transferred to the more outboard/hinterland Eidsfjord detachment, which cut down-section across the former shear zone at roughly 404 Ma. We are not aware of any Devonian detachment resurfacing in Lofoten to the west of Eidsfjord, implying that those rocks reside in the upper plate of the Eidsfjord detachment. Given the strong Permian overprint recorded in rocks underlying the more outboard islands of the Lofoten archipelago, one cannot rule out that remnants of a Devonian detachment may be present there, if not completely excised (Steltenpohl et al., 2004). The sporadic preservation of pre-Scandian, Middle-Ordovician metamorphic structures and fabrics in more inboard parts of Lofoten (Steltenpohl et al., 2003a, 2011; Corfu, 2004; Mager, 2005) is compatible with an upper-plate setting. We interpret that the Eidsfjord detachment itself was eventually abandoned some time after the Early Devonian, having been excised at depth by the tops-east detachment along the eastern flank of the Permian Lofoten core complex (Steltenpohl et al., 2004).

Our understanding of the Permian and later development of the Norwegian margin presently is based primarily on the wealth of offshore geophysical and drill core data provided by petroleum companies exploring along the continental shelf (Brekke and Riis, 1987; Blystad et al., 1995; Løseth and Tveten, 1996; Olesen et al., 1997, 2002; Brekke, 2000; Tsikalas et al., 2001, 2005, 2008; Wilson et al., 2005, 2006; Bergh et al., 2007; Hansen, 2009). The submerged Lofoten–Vesterålen shelf preserves a good sedimentary rock record dating from the Permian into the Tertiary that brackets periods of extensional fault movements. Bergh et al. (2007) synthesized this offshore information and used onshore lineament analyses coupled with ground-truthing to formulate groupings of fractures which they projected across Lofoten–Vesterålen. The only onshore occurrence of post-Caledonian sedimentary rocks in Lofoten–Vesterålen, however, is a small fragment of an isolated Jurassic basin exposed on Andøy (just north of the area of Fig. 2: Dalland, 1975). Our approach coming from onshore, therefore, is different, as it relies on field observations first to establish the relative sequencing of faults and then, where possible, applying isotopic age dating methods to bracket the absolute timing of faulting episodes. Cross section B–B′ (Fig. 4) melds an offshore seismic interpretation from Bergh et al. (2007) to the onshore section that we have mapped (see Fig. 2 for the line of section B–B′). The timing we suggest for faults in Fig. 4 broadly follows that of Bergh et al. (2007), but we caution that episodes of faulting offshore may not necessarily correspond one-to-one to episodes on the mainland. For example, Steltenpohl et al. (2009) report evidence for Middle Triassic faulting related to the widening of the Vestfjord basin (Fig. 2), which has no other known counterpart in Lofoten–Vesterålen but is common on the conjugate side of the orogen in East Greenland. “Mesozoic faults” depicted in Fig. 15, therefore, are those that we have either directly dated or correlated to dated ones, including those in the Jurassic Sortlandsund basin, based on field relations, and they tend to have westerly dips. “Mesozoic-Tertiary faults”, on the other hand, cut across or reactivate the Mesozoic faults, generally have higher degrees of hydrothermal alteration than was observed for the older Mesozoic faults, and they have subvertical dips (Figs. 4 and 15). Our interpretation of the timing of the post-Permian faults also derives from consideration of the results of apatite fission track dates from across Lofoten–Vesterålen presented in Hendriks et al. (2010).

All three of brittle and brittle-ductile faults and/or shears from the Fiskefjord area that we dated using $^{40}Ar/^{39}Ar$ on K-feldspar record Mesozoic tops-west normal movements. These dates are compatible with the presence of the Jurassic Sortlandsund basin, toward which each of the faults and shears dip. In Fig. 4 we infer that these faults shallow at depth and root into a substantial Mesozoic detachment formed beneath the Sortlandsundet basin. This interpretation stems mainly from the map relations and geometries of the numerous low-angle, westward-dipping Mesozoic shear zones found around Fiskefjord (Figs. 3 and 11A), and it provides a supradetachment mechanism for formation of the Sortlandsund basin. Though our understanding of the kinematics and absolute timing of the basal Fiskefjord shear zone is relatively limited, it displays evidence for multiple pulses of reactivation. The earliest-formed and most abundant mylonites within the zone have a tops-east thrust geometry, whereas local overprinting tops-west mylonitic shears (Fig. 11C) have a rheology and kinematics that resemble those we have described for the extensional Devonian Eidsfjord shear zone. Combined with its unique association with abundant pseudotachylites, we interpret that the Fiskefjord shear zone also records Devonian tops-west extensional movement. Taken together, it appears that the Fiskefjord shear zone initiated as a Scandian (Silurian) basement-on-basement thrust that was reactivated during Devonian tops-west extensional movements, and then reactivated again as a tops-west Mesozoic normal fault (Fig. 4). Farther west along B–B′ (Fig. 4), we infer that the faults beneath Eidsfjord, including the Eidsfjord fault zone (Fig. 3) of Hendriks et al. (2010), are of Mesozoic age based on their similar geometries.

High-angle, Mesozoic and Tertiary normal faults further cut the Fiskefjord shear zone, and are well documented along the flanks of the Lofoten and Utrøst ridges and Vestfjorden (Løseth and Tveten, 1996; Steltenpohl et al., 2004; Bergh et al., 2007). While our relatively higher temperature $^{40}Ar/^{39}Ar$ thermochonometers (muscovite and K-feldspar closure temperatures ~350 °C and ~250 °C, respectively) help to constrain the Mesozoic and earlier exhumation history of Lofoten–Vesterålen, they do not appear to be sensitive to the effects of Tertiary to Modern exhumation, the latter of which is best documented by the apatite fission track dates of Hendriks et al. (2010) and studies of geomorphic contrasts developed across these younger faults (Osmundsen et al., 2010).

Bergh et al. (2007) suggested that the Hadselfjord fault zone (Fig. 3) connects to the Late Cretaceous Western Lofoten border fault, which is supported by the apatite fission track dates. Combined with our field and $^{40}Ar/^{39}Ar$ investigation of breccia from the Rødsand fault (Fig. 3), we interpret movement having initiated in the Late Triassic to Early Jurassic with reactivation occurring later in the Cretaceous and possibly continuing into the Tertiary (Davids et al., 2010); this fault is, therefore, shown as a Mesozoic-Tertiary fault in Fig. 4.

5.2. Significance for Devonian extension in northern Norway

The Eidsfjord detachment has structural and temporal similarities to other syn- to post-orogenic extensional systems exposed in mid-to-southwestern Norway. The Early to Middle Devonian timing, low-angle and hinterland-dipping geometry, tops-west kinematics, segmentation by syn-extensional strike-slip and later brittle faults, and west-plunging scoop-shaped geometry all corroborate that the Eidsfjord detachment is a northern counterpart to the Nordfjord–Sogn and other faults of the system of Devonian detachments (Fig. 1). Our work farther north of Lofoten, up to latitude 70° N, implies that the Eidsfjord detachment is the most northern segment of the Devonian extensional detachment system exposed in Scandinavia (Fig. 1).

There are several characteristics of the Eidsfjord system, however, that distinguish it from the Nordfjord–Sogn detachment system. In contrast to western Norway, Devonian sedimentary

basins are nowhere known to be preserved in the Lofoten–Vesterålen region. Olesen et al. (2002) and Wilson et al. (2006) used mostly geophysical information to infer SW-plunging "spoon-shaped depressions" paralleling and flanking the Lofoten ridge, and hypothesized that they formed during the Devonian. Although no absolute timing measurements were reported to support their hypothesis, the same authors inferred that the depressions are geometrically similar to the Devonian basins of west Norway. The average elongation lineation for the Eidsfjord detachment is N72°W, which is ~35° to the extension direction in west and central Norway (Braathen et al., 2002), parallels corregations in the detachment surface and these make a high angle to the Lofoten ridge, nearly orthogonal to the inferred direction of transport based on geophysics (Olesen et al., 2002). They also extrapolated Bugge et al.'s (2002) interpretation that Upper Permian-Lower Triassic sandstones deposited offshore of mid-Norway (~1000 km south of Lofoten) "…probably represent reworking of older [Upper Devonian-Lower Permian] sedimentary rocks present to the east …" Substantial volumes of Permian-Lower Triassic clastics occur along the Lofoten shelf, and post- Permo-Triassic uplift and erosion has likely contributed to the further removal of earlier-formed Devonian basins. Permo-Triassic inversion of former Devonian basins has been suggested to explain the lack of Devonian sediments along the Lofoten shelf (Sherlock, 2001), though inversion is not required by the data (Steltenpohl et al., 2004). In East Greenland, where the post-Early Carboniferous and Permian basins are subaerially exposed, we see no evidence to support inversion of the Devonian basins (Larsen et al., 2008; Olsen, 1993; Stemmerik et al., 1993).

The Eidsfjord shear zone is developed fully *within* basement, not at or near a basement-Devonian cover or basement-Scandian allochthon contact as in central and southwestern Norway (Andersen and Jamtveit, 1990; Braathen, 1999). The shear zone does, however, appear to root beneath the Leknes thrust (Tull, 1978; Klein and Steltenpohl, 1999; Klein et al., 1999), which recent work implies is a pre-Scandian structure (Corfu, 2004; Steltenpohl et al., 2010a, 2010b, 2011).The zone of ductile deformation within the Eidsfjord shear zone is considerably thinner than the detachments to the south (200 m vs. kilometers). Thus, considering its thickness, the Eidsfjord detachment appears to be more similar to shear zones along the western flanks of the Gneiss windows to the south; for example, shear zones bordering the Nasafjell and Børgefjell windows (Fig. 1) have structural thicknesses of ca. 50–200 m, and the Nesna shear zone is up to ~1 km (Osmundsen et al., 2003). The Eidsfjord shear zone also has neither the magnitude of heave nor throw required for the Nordfjord–Sogn detachment. Pressure estimates from recrystallized assemblages in mylonites from the Eidsfjord detachment document a minimum depth of ~35 km for initiation of normal movement (Moecher and Steltenpohl, 2009, 2011). In contrast with lower-plate eclogites in the Nordfjord–Sogn detachment, we interpret the Eidsfjord detachment to project southwestward beneath the eclogite terrane exposed on Flakstadøy (Steltenpohl et al., 2010b, 2011). An upper-plate geometry is compatible with other Middle-Ordovician relics in Lofoten, including the 457 Ma muscovite cooling date for sample HU-2 reported herein. Pressure-temperature estimates for the Flakstadøy eclogites are also much lower than those for the Western Gneiss Region (14–15 kbar 680 °C versus ≤40 kbar 750–800 °C, respectively), but are more similar to those reported for the allochthonous Seve, Tromsø, and Bergen Arcs eclogite-facies allochthons (Steltenpohl et al., 2003a, 2011).

Permian $^{40}Ar/^{39}Ar$ mineral cooling dates from the Lofoten ridge coupled with Permian siliciclastic basins along the submerged shelf led Steltenpohl et al. (2004) to suggest that Permian, rather than Devonian, extension in the North was much more pervasive than it was in western Norway. The Devonian detachment in western Lofoten apparently remained tectonically buried at a depth beneath the ~350 °C isotherm (i.e., muscovite closure with respect to $^{40}Ar/^{39}Ar$) more than 100 m.y. after the Nordfjord–Sogn detachment was exhumed through the same thermocrustal level. Intense retrogression of the Lofoten eclogites also is consistent with longer residency within the evolving orogenic core than lower plate rocks exposed today in the Western Gneiss Region (Steltenpohl et al., 2006, 2011). The northernmost segment of the Devonian detachment system differs also in that it is the most proximal low-angle ductile normal fault to the Norwegian continental-oceanic boundary (Osmundsen et al., 2002). In our study area, the Eidsfjord shear zone appears to be severely chopped by Permian detachments and higher-angle normal faults of the Vanna-Vestfjord fault complex (Figs. 3 and 4), by Mesozoic rift faults, and finally by Eocene faults that resulted in continental separation (Steltenpohl et al., 2004, 2009, herein; Wilson et al., 2006; Bergh et al., 2007).

Crustal-scale seismic sections for the mid-Norway passive margin show numerous low-angle normal detachment faults with 20–40 km offsets bounding blocks of rotated continental crust (Osmundsen and Ebbing, 2008). Some of the proximal blocks and faults on interpreted seismic sections display a geometry typical of metamorphic core complexes. Osmundsen et al. (2002) and Osmundsen and Ebbing (2008) contend that localization of the southeast rifted margin was controlled by a pre-existing, antiformal core complex inherited from Paleozoic, large-magnitude extension. We propose that the Eidsfjord–Fiskfjord shear zone system is part of an exhumed, onshore analog of one of these seismically imaged metamorphic core complex bounding structures. The Eidsfjord detachment is directly along strike to the northeast of the Vøring Basin rifted margin examined by Osmundsen and Ebbing (2008). Section B–B′ in Fig. 4 illustrates several large ramp-flat geometry, rotated extensional fault blocks, one in the east and one in the middle underlain respectively by Mesozoic and Permian detachments that resemble those in Osmundsen and Ebbing's (2008) offshore seismic sections. Although our time-slice sections in Fig. 15 do not emphasize merging of the detachment shear zones through time, we imagine that later core complexes formed progressively outboard as the Norwegian margin continued to extend and thin, with the later-formed extensional shear zones exploiting the anisotropies developed during the Devonian and Permian core complex formation. In addition to the appropriate geometric and kinematic patterns, the Eidsfjord shear zone exhibits pervasive evidence of fluid infiltration common to metamorphic core complexes (Kerrich and Hyndman, 1986; Fricke et al., 1992; Moecher and Steltenpohl, 2011). The Eidsfjord shear zone, therefore, appears to be an exposed analog of subsurface detachments inferred in offshore seismic lines (Osmundsen and Ebbing, 2008; Tsikalas et al., 2008).

Finally, the plethora of pseudotachylyte veins associated with the Eidsfjord–Fiskefjord shear zone distinguishes it from the Nordfjord–Sogn detachment. Bergh et al. (2007; Figs. 11 and 15, and Table 1) show the Eidsfjord shear zone as an "S2" lineament ("normal faults and extensional fractures"), which are characterized by a down-to-the-NNW or -SSE motion, and mainly semi-brittle deformation, including formation of pseudotachylyte. Bergh et al. (2007) invoke Permo-Jurassic proto-rifting on east-dipping crustal-scale detachments as the initial phase of extension. Our measured extension direction for the ductile Eidsfjord shear zone is WNW, however, and our thermochronology demonstrates that ductile extension had initiated during the Early Devonian, well before Permian times, so both the kinematics and the timing are compatible with that reported for the Mid-Norway rifted margin (Osmundsen et al., 2002). Pseudotachylyte generation within the Eidsfjord–Fiskefjord shear zone occurred primarily during deformation well below the conventional brittle-ductile transition,

documenting that it was seismically active during its ductile history (Moecher and Steltenpohl, 2009, 2011). We cannot constrain magnitude of seismicity as yet because we have not mapped out in detail the distribution of the pseudotachylytes. Abundant pseudotachylyte generation in a ductile normal fault with a low dip angle (~30°) like the present-day Eidsfjord–Fiskefjord shear zone, implies periodic strengthening sufficient for coseismic slip. Given the present-day low-angle dip and other similarities with the Nordfjord–Sogn detachment, the surface geologic relations that resulted in cross section C–C′ in Fig. 4, offshore seismic surveys from Mid-Norway indicating that the last phase of normal displacement is clearly very low angle to horizontal, and the fact that some pseudotachylytes we measured also cut the low-angle mylonites (Moecher and Steltenpohl, 2009, 2011), we interpret that the Eidsfjord–Fiskefjord shear zone formed as a low-angle normal fault. Although active seismogenic low-angle normal faults are now recognized (Abers et al., 1997; Brozzetti et al., 2009), the simplest explanation for the low dip of the Eidsfjord–Fiskefjord shear zone is that it represents a reactivated Caledonian thrust. We see only minor evidence for an early thrust history, but if reactivation occurred then original thrust structures could have been obliterated. As the Eidsfjord–Fiskefjord shear zone is marked by a lithologic contact, it is also possible that the shear zone took advantage of slight strength contrasts between two crystalline rock types. If fault reactivation did not occur, and the Eidsfjord shear zone is a newly formed rupture, then special conditions for failure in these strong crystalline rocks must have developed. This has implications for (1) the strength of and a mechanism for seismicity in lower crust and (2) for behavior of low-angle normal faults that have been debated as to whether they are seismogenic.

Acknowledgments

A MGS wishes to thank Michael Kunk for help in assisting in the $^{40}Ar/^{39}Ar$ step-heating analyses using U.S.G.S. laboratory facilities in Reston, VA. The UK EPMA is supported by NSF grant EAR 0824714; field work for DM was funded by a Faculty Support Grant from the University of Kentucky. JB thanks the Geological Society of America for a graduate student grant-in-aid award to support this research and he and SM thank the G.S.A. and the College of Science and Mathematics, Auburn University, for grants to support travel for presentations at annual meetings of the G.S.A. The authors wish to thank Auburn University students Thomas Key and Wes Buchanan for their geologic mapping contributions to this research.

Appendix 1.

$^{40}Ar/^{39}Ar$ analytical data and UTM locations for muscovite samples from the Eidsfjord detachment fault; Auburn Nobel Isotope Mass Analytical Laboratory (ANIMAL).

Date Run:	4/29/08		
Volts ^{40}Ar from air:	#DIV/0!		
Irradiation Package:	AU-11		
Date of Irradiation:	4/29/2008		
Air $^{40}Ar/^{36}Ar$:	293.0	+	1.5

n	^{40}Ar (*+atm)	Error	^{39}Ar(K)	Error	^{38}Ar (Cl + atm)	Error	^{37}Ar(Ca)	Error	^{36}Ar (atm)	Error	%rad	R	Age (Ma)	Error
51	2.650E-14	2.42E-17	1.534E-15	7.16E-18	3.02E-18	5.79E-20	7.5E-18	6.52E-19	3.42E-19	7.52E-20	99.6%	17.2041	406.2	2.0
52	5.452E-14	3.62E-17	3.076E-15	4.63E-18	7.53E-18	9.04E-20	−1.3E−18	4.67E-19	3.41E-18	9.88E-20	98.2%	17.3997	410.4	0.7
53	1.448E-14	1.18E-17	8.122E-16	1.92E-18	1.92E-18	7.90E-20	−5.6E−19	4.92E-19	8.47E-19	8.22E-20	98.3%	17.5154	412.8	1.3
54	2.152E-14	2.17E-17	1.209E-15	3.11E-18	2.86E-18	8.34E-20	−3.8E−20	4.74E-19	1.73E-18	1.01E-19	97.6%	17.3697	409.7	1.3
55	6.306E-14	3.56E-17	3.422E-15	3.64E-18	1.05E-17	1.30E-19	5.5E-18	6.16E-19	1.23E-17	1.63E-19	94.2%	17.3673	409.7	0.6
56	4.892E-14	2.11E-17	2.815E-15	5.36E-18	6.46E-18	6.41E-20	3.7E-18	5.36E-19	3.67E-19	1.01E-19	99.8%	17.3410	409.1	0.8
57	6.552E-14	5.13E-17	3.679E-15	4.11E-18	8.18E-18	1.40E-19	1.7E-17	7.89E-19	2.41E-18	9.76E-20	98.9%	17.6183	415.0	0.6
58	1.704E-14	1.68E-17	9.818E-16	6.13E-18	2.19E-18	6.05E-20	1.3E-18	6.61E-19	4.91E-19	8.66E-20	99.1%	17.2045	406.2	2.7
59	2.844E-14	2.98E-17	1.671E-15	5.72E-18	4.13E-18	6.96E-20	2.9E-17	5.41E-19	−1.5E−19	−1.8E−19	100.2%	17.0472	402.9	1.6
60	1.259E-13	4.88E-17	6.397E-15	1.34E-17	1.74E-17	1.85E-19	2.3E-16	2.16E-18	3.65E-18	1.51E-19	99.1%	19.5091	454.3	1.0

au11.4g.mus: **JB07-87A/2 UTM 7608087 0547649**.
Mean = 410.9 ± 2.4 [0.58%] 95% conf.
Wtd by data-pt errs only, 1 of 10 rej.
MSWD = 11.4, probability = 0.000.
*means radiogenic.

n	^{40}Ar (*+atm)	Error	^{39}Ar(K)	Error	^{38}Ar (Cl + atm)	Error	^{37}Ar(Ca)	Error	^{36}Ar (atm)	Error	%rad	R	Age (Ma)	Error
61	6.344E-14	6.45E-17	3.649E-15	7.09E-18	8.72E-18	9.70E-20	2.34E-18	6.09E-19	2.93E-18	1.21E-19	98.6%	17.1482	405.1	0.9
62	1.113E-13	2.18E-16	6.452E-15	1.57E-17	1.54E-17	1.30E-19	7.67E-16	3.96E-18	7.12E-19	7.98E-20	99.8%	17.2121	406.4	1.3
63	9.593E-14	7.00E-17	5.532E-15	1.04E-17	1.52E-17	2.01E-19	1.88E-16	3.05E-18	2.49E-18	1.69E-19	99.2%	17.2094	406.3	0.9
64	2.089E-14	2.40E-17	1.220E-15	5.76E-18	2.90E-18	8.02E-20	4.61E-17	8.49E-19	1.04E-19	6.74E-20	99.9%	17.1034	404.1	2.0
65	3.649E-14	4.59E-17	2.102E-15	4.24E-18	4.68E-18	7.26E-20	1.43E-16	1.06E-18	2.23E-19	8.25E-20	99.8%	17.3301	408.9	1.0
66	5.077E-14	2.30E-17	2.890E-15	8.83E-18	7.54E-18	1.19E-19	1.19E-16	1.19E-18	2.84E-18	1.12E-19	98.3%	17.2775	407.8	1.3
67	2.926E-14	2.93E-17	1.703E-15	2.84E-18	3.59E-18	7.46E-20	7.05E-17	5.11E-19	3.14E-19	8.40E-20	99.7%	17.1229	404.5	0.9
68	9.993E-14	2.72E-17	5.835E-15	1.41E-17	1.45E-17	1.23E-19	3.21E-16	3.72E-18	1.13E-18	1.12E-19	99.7%	17.0691	403.4	1.0
69	3.402E-14	3.76E-17	1.965E-15	8.66E-18	5.38E-18	5.75E-20	1.20E-16	7.20E-19	8.07E-19	7.11E-20	99.3%	17.1921	406.0	1.9
70	2.794E-14	2.46E-17	1.583E-15	4.32E-18	4.54E-18	8.01E-20	7.24E-18	7.03E-19	2.53E-18	1.14E-19	97.3%	17.1722	405.6	1.3

au11.6h.mus: **TK07-37 UTM 0547651 7607655**.
Mean = 405.8 ± 1.2 [0.30%] 95% conf.
Wtd by data-pt errs only, 0 of 10 rej.
MSWD = 2.4, probability = 0.011.

n	^{40}Ar (*+atm)	Error	^{39}Ar(K)	Error	^{38}Ar (Cl + atm)	Error	^{37}Ar(Ca)	Error	^{36}Ar (atm)	Error	%rad	R	Age (Ma)	Error
61	4.664E-14	1.84E-17	2.651E-15	1.49E-18	6.28E-18	6.87E-20	2.42E-16	1.56E-18	5.93E-19	6.77E-20	99.6%	17.5264	409.9	0.3
62	5.589E-14	4.43E-17	2.124E-15	3.49E-18	5.96E-18	8.28E-20	2.59E-15	5.30E-18	2.14E-18	8.13E-20	98.9%	26.0125	579.3	1.1
63	5.870E-14	7.89E-17	3.303E-15	3.01E-18	8.56E-18	6.90E-20	2.66E-16	2.15E-18	1.88E-18	8.56E-20	99.1%	17.6015	411.5	0.7
64	8.246E-15	8.70E-18	4.459E-16	1.20E-18	8.50E-19	2.51E-20	1.22E-17	2.60E-19	2.21E-19	7.72E-20	99.2%	18.3441	426.9	1.7
65	1.024E-13	5.47E-17	1.726E-15	3.40E-18	6.32E-18	1.58E-19	7.35E-16	3.46E-18	7.98E-18	1.83E-19	97.7%	57.9572	1103.6	2.4
66	8.209E-14	7.55E-17	4.520E-15	4.64E-18	1.13E-17	1.36E-19	3.94E-16	2.54E-18	2.00E-18	1.04E-19	99.3%	18.0324	420.5	0.6
67	1.331E-14	6.20E-18	7.549E-16	1.85E-18	1.91E-18	5.53E-20	9.18E-18	6.17E-19	4.63E-19	8.26E-20	99.0%	17.4475	408.3	1.3
68	1.263E-14	1.08E-17	7.05E-16	9.64E-19	1.5E-18	2.46E-20	2.4E-16	1.7E-18	1.3E-19	5.6E-20	99.7%	17.8639	417.0	1.1
69	1.485E-14	1.20E-17	2.89E-16	2.53E-18	1.3E-18	3.03E-20	8.8E-17	1.1E-18	7.7E-19	7.4E-20	98.5%	50.6949	997.0	9.06
70	2.260E-15	6.38E-18	6.959E-17	7.02E-19	1.3E-19	2.6E-20	6.5E-16	2.3E-18	1E-19	2.7E-20	98.7%	32.0509	690.8	10.1

au11.4c.mus: **JB07-82A UTM 7614739 058339**.
Mean = 429 ± 62 [14%] 95% conf.
Wtd by data-pt errs only, 0 of 10 rej.
MSWD = 11,859, probability = 0.000.

n	^{40}Ar (*+atm)	Error	^{39}Ar(K)	Error	^{38}Ar (Cl + atm)	Error	^{37}Ar(Ca)	Error	^{36}Ar (atm)	Error	%rad	R	Age (Ma)	Error
81	1.126E-14	8.05E-18	5.451E-16	3.25E-18	1.36E-18	4.95E-20	3.22E-16	3.36E-18	6.91E-19	6.17E-20	98.2%	20.2811	466.6	3.0
82	5.684E-14	2.84E-17	3.107E-15	2.69E-18	7.13E-18	6.67E-20	1.74E-15	3.43E-18	1.87E-18	6.58E-20	99.0%	18.1175	422.2	0.5
83	1.042E-13	6.11E-17	2.648E-15	8.10E-18	8.55E-18	1.53E-19	3.09E-15	7.86E-18	6.04E-18	1.38E-19	98.3%	38.6628	805.4	2.6
84	4.107E-14	1.82E-17	8.389E-16	3.91E-18	2.33E-18	7.39E-20	3.85E-16	3.82E-18	1.84E-18	8.70E-20	98.7%	48.3060	960.6	4.6
85	7.549E-14	5.94E-17	3.065E-15	1.15E-17	8.25E-18	1.47E-19	4.86E-15	1.47E-17	2.20E-18	7.62E-20	99.1%	24.4152	548.6	2.1
86	1.202E-13	7.66E-17	6.522E-15	8.51E-18	1.53E-17	1.30E-19	8.95E-16	4.79E-18	2.91E-18	1.15E-19	99.3%	18.2957	425.9	0.6
87	9.508E-15	9.18E-18	5.129E-16	1.56E-18	1.68E-18	5.82E-20	1.62E-17	5.67E-19	1.04E-18	7.16E-20	96.8%	17.9393	418.5	1.7
88	1.856E-14	1.56E-17	4.314E-16	1.73E-18	9.42E-19	3.75E-20	1.34E-15	3.90E-18	6.44E-19	4.53E-20	99.0%	42.5852	870.2	3.7
89	3.586E-14	1.91E-17	1.982E-15	4.42E-18	5.93E-18	1.39E-19	8.79E-16	4.45E-18	5.30E-19	5.90E-20	99.6%	18.0128	420.1	1.0
90	1.898E-14	1.32E-17	9.933E-16	2.16E-18	2.69E-18	4.36E-20	3.11E-16	1.77E-18	1.08E-18	7.41E-20	98.3%	18.7828	436.0	1.2

au11.4e.mus: **TK07-33 UTM 5038111 7614519**.
Mean = 439 ± 55 [12%] 95% conf.
Wtd by data-pt errs only, 0 of 10 rej.
MSWD = 5708, probability = 0.000.

n	^{40}Ar (*+atm)	Error	^{39}Ar(K)	Error	^{38}Ar (Cl + atm)	Error	^{37}Ar(Ca)	Error	^{36}Ar (atm)	Error	%rad	R	Age (Ma)	Error
91	1.089E-13	5.32E-17	6.112E-15	1.43E-17	1.65E-17	1.99E-19	3.95E-17	6.97E-19	8.26E-18	1.89E-19	97.8%	17.4166	407.6	1.0
92	1.259E-13	9.43E-17	7.022E-15	4.38E-18	1.83E-17	1.83E-19	2.11E-17	8.46E-19	7.88E-18	1.86E-19	98.2%	17.5937	411.3	0.4
93	3.341E-14	2.02E-17	1.865E-15	4.30E-18	5.63E-18	1.01E-19	1.14E-18	3.57E-19	2.82E-18	8.04E-20	97.5%	17.4611	408.5	1.0
94	1.284E-13	5.09E-17	7.236E-15	1.02E-17	1.78E-17	1.29E-19	7.02E-16	4.15E-18	1.31E-18	9.26E-20	99.7%	17.6852	413.2	0.6
95	1.744E-13	1.36E-16	9.651E-15	9.55E-18	2.50E-17	2.54E-19	3.26E-16	1.81E-18	5.60E-18	1.52E-19	99.1%	17.9004	417.7	0.5
96	1.939E-13	1.83E-16	1.106E-14	9.23E-18	2.76E-17	1.75E-19	4.19E-17	1.13E-18	1.67E-18	1.14E-19	99.7%	17.4933	409.2	0.5
97	7.232E-14	3.62E-17	4.005E-15	6.69E-18	1.14E-17	1.19E-19	8.04E-18	4.27E-19	6.18E-18	1.49E-19	97.5%	17.5988	411.4	0.8
98	6.006E-14	8.56E-17	3.357E-15	4.52E-18	8.71E-18	1.17E-19	2.73E-18	3.74E-19	5.16E-18	1.18E-19	97.5%	17.4366	408.0	0.9
99	2.488E-14	1.45E-17	1.409E-15	3.19E-18	4.26E-18	5.15E-20	4.22E-18	4.34E-19	8.84E-19	6.83E-20	98.9%	17.4752	408.8	1.0
100	1.972E-13	6.30E-17	1.120E-14	1.23E-17	2.60E-17	2.40E-19	7.29E-17	1.45E-18	3.18E-18	1.35E-19	99.5%	17.5267	409.9	0.5

au11.4f.mus: **JB07-90 UTM 7607871 0547634**.
Mean = 410.3 ± 1.3 [0.31%] 95% conf.
Wtd by data-pt errs only, 1 of 10 rej.

Appendix 2.

Tabulated results of the ^{40}Ar/^{39}Ar analyses.

Sample = SM-21A Muscovite

J = 0.012284 ± 0.50% Sample wt. = 0.0020 g

Temp °C	Initial and radiogenic ^{40}Ar	Potassium-derived ^{39}Ar	Chlorine-derived ^{38}Ar	Calcium-derived ^{37}Ar	Initial ^{36}Ar	Age* in Ma	**
650	6.817×10^{-14}	2.601×10^{-15}	3.009×10^{-15}	3.204×10^{-16}	***	391.68	±8.86
750	2.921×10^{-13}	1.210×10^{-14}	***	1.935×10^{-16}	***	459.28	±1.61
850	9.024×10^{-13}	3.520×10^{-14}	***	3.224×10^{-16}	***	490.50	±0.52
950	8.358×10^{-12}	2.648×10^{-13}	8.362×10^{-15}	6.893×10^{-16}	***	589.48	±0.21
1000	2.072×10^{-12}	7.142×10^{-14}	2.151×10^{-15}	6.483×10^{-16}	***	548.59	±0.36
1050	4.183×10^{-12}	1.391×10^{-13}	4.362×10^{-15}	7.394×10^{-16}	***	565.99	±0.18
1250	4.472×10^{-12}	1.413×10^{-13}	4.766×10^{-15}	1.881×10^{-16}	***	591.12	±0.22
1450	1.730×10^{-13}	3.758×10^{-15}	***	8.791×10^{-16}		793.76	±4.11
Total	2.052×10^{-11}	6.703×10^{-13}	2.472×10^{-15}	5.674×10^{-15}	3.067×10^{-15}	573.76	
No Plateau.							

v 8/23/93	Sample = SM127 Muscovite						10:00:01 4 Sept 1980
$J = 0.012316 = 0.50\%$					Sample wt. = 0.0019 g		
Temp °C	Initial and radiogenic ^{40}Ar	Potassium-derived ^{39}Ar	Chlorine-derived ^{38}Ar	Calcium-derived ^{37}Ar	Initial ^{36}Ar	Age* in Ma	**
650	6.903×10^{-14}	2.106×10^{-15}	1.074×10^{-15}	3.238×10^{-16}	***	388.13	±15.65
750	2.093×10^{-13}	7.513×10^{-15}	***	5.925×10^{-16}	***	522.92	±2.89
800	2.081×10^{-13}	7.486×10^{-15}	***	***	***	523.19	±3.45
850	6.178×10^{-13}	1.961×10^{-14}	***	1.989×10^{-16}	***	585.45	±0.88
900	4.209×10^{-12}	1.379×10^{-13}	***	2.583×10^{-16}	***	573.19	±0.24
950	2.823×10^{-12}	9.561×10^{-14}	***	3.624×10^{-16}	***	557.76	±0.39
1000	1.885×10^{-12}	6.170×10^{-14}	***	3.113×10^{-16}	***	573.15	±0.53
1150	5.200×10^{-12}	1.784×10^{-13}	***	5.170×10^{-16}	***	551.59	±0.21
Total	1.522×10^{-11}	1.513×10^{-13}	1.284×10^{-15}	2.688×10^{-15}	3.503×10^{-16}	561.05	

Plateaus: 92.8% of gas on plateau, steps 950 °C–1200 °C, plateau age = 375.48 ± 1.7 Ma

v 9/29/99	Sample = SM127 Muscovite						15:45:53 23 Jan 1980
$J = 0.009844 = 0.50\%$					Sample wt. = 0.0112 g		
Temp °C	Initial and radiogenic ^{40}Ar	Potassium-derived ^{39}Ar	Chlorine-derived ^{38}Ar	Calcium-derived ^{37}Ar	Initial ^{36}Ar	Age* in Ma	**
850	9.114×10^{-13}	3.468×10^{-14}	5.473×10^{-16}	5.854×10^{-16}	***	501.73	±0.71
950	4.609×10^{-12}	1.693×10^{-13}	9.031×10^{-16}	7.587×10^{-16}	***	520.77	±0.31
1050	2.487×10^{-12}	9.269×10^{-14}	9.060×10^{-16}	8.520×10^{-16}	***	514.26	±0.39
1150	3.320×10^{-12}	1.190×10^{-13}	6.550×10^{-16}	4.538×10^{-16}	***	531.96	±0.32
1250	1.111×10^{-12}	3.729×10^{-14}	2.257×10^{-16}	1.018×10^{-16}	***	561.84	±1.01
Total	1.244×10^{-11}	4.503×10^{-13}	4.344×10^{-15}	3.668×10^{-15}	2.263×10^{-16}	524.36	

v 4/3/99	Sample = SM92A Muscovite						15:32:02 23 Jan 1980
$J = 0.012306 = 0.50\%$					Sample wt. = 0.0020 g		
Temp °C	Initial and radiogenic ^{40}Ar	Potassium-derived ^{39}Ar	Chlorine-derived ^{38}Ar	Calcium-derived ^{37}Ar	Initial ^{36}Ar	Age* in Ma	**
550	2.152×10^{-13}	2.168×10^{-15}	6.529×10^{-16}	2.364×10^{-16}	2.796×10^{-16}	385.90	±8.83
650	6.214×10^{-14}	3.005×10^{-15}	4.350×10^{-16}	2.815×10^{-16}	***	319.96	±8.09
750	2.118×10^{-13}	9.412×10^{-15}	3.990×10^{-16}	2.142×10^{-16}	***	434.21	±1.93
850	7.855×10^{-13}	3.635×10^{-14}	6.937×10^{-16}	3.103×10^{-16}	***	421.23	±0.74
950	7.512×10^{-12}	3.253×10^{-13}	1.602×10^{-15}	1.287×10^{-16}	***	449.85	±0.16
1050	2.430×10^{-12}	1.039×10^{-13}	1.433×10^{-15}	3.398×10^{-16}	***	454.37	±0.31
1150	4.601×10^{-12}	2.204×10^{-13}	8.669×10^{-16}	3.533×10^{-16}	***	411.82	±0.20
1250	4.630×10^{-13}	2.045×10^{-14}	***	2.606×10^{-16}	***	440.59	±1.05
1450	1.085×10^{-13}	1.995×10^{-15}	***	***	***	890.76	±7.32
Total	1.639×10^{-11}	7.231×10^{-13}	6.216×10^{-15}	3.385×10^{-15}	8.520×10^{-16}	437.76	

v 4/3/99	Sample = HU2 Muscovite						15:55:46 23 Jan 1980
$J = 0.012309 = 0.50\%$					Sample wt. = 0.0022 g		
Temp °C	Initial and radiogenic ^{40}Ar	Potassium-derived ^{39}Ar	Chlorine-derived ^{38}Ar	Calcium-derived ^{37}Ar	Initial ^{36}Ar	Age* in Ma	**
550	1.862×10^{-13}	1.891×10^{-15}	5.699×10^{-16}	1.056×10^{-16}	5.563×10^{-16}	398.54	±20.34
650	7.085×10^{-14}	2.681×10^{-15}	***	5.699×10^{-16}	***	398.46	±13.41
750	3.264×10^{-13}	1.335×10^{-14}	***	5.699×10^{-16}	***	396.99	±2.09
850	1.533×10^{-12}	6.198×10^{-14}	***	5.699×10^{-16}	***	396.99	±0.58
950	9.107×10^{-12}	3.851×10^{-13}	3.753×10^{-16}	5.699×10^{-16}	2.230×10^{-16}	397.99	±0.18
1050	6.804×10^{-12}	2.896×10^{-13}	2.845×10^{-16}	5.699×10^{-16}	1.475×10^{-16}	401.01	±0.19
1100	5.821×10^{-13}	2.460×10^{-14}	***	5.699×10^{-16}	***	397.88	±1.22
1150	2.676×10^{-13}	1.121×10^{-14}	***	5.699×10^{-16}	***	397.26	±2.84
1200	2.260×10^{-13}	9.365×10^{-15}	***	5.699×10^{-16}	***	394.72	±3.29
1250	1.890×10^{-13}	7.796×10^{-15}	***	5.699×10^{-16}	***	394.14	±5.01
1350	2.218×10^{-13}	9.375×10^{-15}	***	5.699×10^{-16}	***	395.10	±4.26
1450	1.733×10^{-13}	7.077×10^{-15}	***	***	***	396.80	±4.25
Total	1.969×10^{-11}	8.240×10^{-13}	1.732×10^{-15}	4.194×10^{-15}	1.307×10^{-15}	398.00	

v 4/3/99	Sample = SM135B Potassium Feldspar						11:37:38 25 Jan 1980
$J = 0.012320 = 0.50\%$					Sample wt. = 0.0020 g		
Temp °C	Initial and radiogenic ^{40}Ar	Potassium-derived ^{39}Ar	Chlorine-derived ^{38}Ar	Calcium-derived ^{37}Ar	Initial ^{36}Ar	Age* in Ma	**
750	4.537×10^{-13}	4.018×10^{-14}	***	2.844×10^{-16}	***	232.12	±0.87
850	1.689×10^{-12}	1.689×10^{-13}	***	6.142×10^{-16}	***	237.65	±0.26
950	2.417×10^{-12}	1.987×10^{-13}	***	1.683×10^{-15}	***	251.24	±0.22
1050	1.610×10^{-12}	1.068×10^{-13}	***	1.112×10^{-15}	***	305.52	±0.38
1150	7.952×10^{-13}	4.236×10^{-14}	***	6.658×10^{-16}	***	371.33	±1.29
1250	3.714×10^{-12}	1.562×10^{-13}	***	2.384×10^{-15}	***	460.11	±0.24
1350	4.796×10^{-12}	2.070×10^{-13}	***	7.740×10^{-16}	***	449.99	±0.41
Total	1.548×10^{-11}	8.986×10^{-12}	2.177×10^{-16}	7.740×10^{-15}	3.547×10^{-16}	344.98	
No Plateau.							

v 4/3/99	Sample = HU2 potassium feldspar						14:00:20 25 Mar 1999
$J = 0.012276 = 0.50\%$					Sample wt. = 0.0020 g		
Temp °C	Initial and radiogenic ^{40}Ar	Potassium-derived ^{39}Ar	Chlorine-derived ^{38}Ar	Calcium-derived ^{37}Ar	Initial ^{36}Ar	Age* in Ma	**
650	1.754×10^{-10}	3.905×10^{-14}	1.814×10^{-15}	***	3.327×10^{-14}	237.70	±1.97
750	4.026×10^{-13}	8.172×10^{-14}	4.572×10^{-15}	***	***	231.21	±0.82
850	6.059×10^{-13}	9.204×10^{-14}	5.715×10^{-15}	***	***	252.20	±0.63
950	6.053×10^{-13}	1.618×10^{-14}	4.910×10^{-15}	***	***	279.56	±4.55
1050	8.046×10^{-13}	3.327×10^{-14}	4.892×10^{-15}	***	***	281.95	±1.52
1150	4.202×10^{-13}	3.327×10^{-14}	2.145×10^{-15}	***	***	281.95	±1.52
1250	2.195×10^{-12}	4.400×10^{-14}	2.612×10^{-15}	3.361×10^{-15}	2.302×10^{-16}	290.89	±0.34
1350	4.693×10^{-12}	1.158×10^{-14}	9.562×10^{-16}	***	8.630×10^{-16}	314.95	±0.46
1450	1.103×10^{-12}	3.786×10^{-14}	5.569×10^{-15}	***	***	323.59	±1.64
1650	6.118×10^{-13}	3.786×10^{-14}	***	***	***	323.59	±1.64
Total	1.162×10^{-11}	9.966×10^{-13}	7.964×10^{-15}	8.645×10^{-15}	3.977×10^{-15}	282.50	
No Plateau.							

v 9/29/99	Sample = Q Potassium Feldspar						15:45:53 23 Jan 1980
$J = 0.009844 = 0.50\%$					Sample wt. = 0.0112 g		
Temp °C	Initial and radiogenic ^{40}Ar	Potassium-derived ^{39}Ar	Chlorine-derived ^{38}Ar	Calcium-derived ^{37}Ar	Initial ^{36}Ar	Age* in Ma	**
850	9.114×10^{-13}	3.468×10^{-14}	5.473×10^{-16}	5.854×10^{-16}	***	501.73	± 0.71
950	4.609×10^{-12}	1.693×10^{-13}	9.031×10^{-16}	7.587×10^{-16}	***	520.77	± 0.31
1050	2.487×10^{-12}	9.269×10^{-14}	9.060×10^{-16}	8.520×10^{-16}	***	514.26	± 0.39
1150	3.320×10^{-12}	1.190×10^{-13}	6.550×10^{-16}	4.538×10^{-16}	***	531.96	± 0.32
1250	1.111×10^{-12}	3.729×10^{-14}	2.257×10^{-16}	1.018×10^{-16}	***	561.84	± 1.01
Total	1.244×10^{-11}	4.503×10^{-13}	4.344×10^{-15}	3.668×10^{-15}	2.263×10^{-16}	524.36	
No Plateau.							

**means error.
***means below detection limit.

References

Abers, G.A., Mutter, C.Z., Fang, J., 1997. Shallow dips of normal faults during rapid extension: earthquakes in the Woodlark-d'Enctrecasteaux rift system, Papua New Guinea. Journal of Geophysical Research 102, 15301–15317.

Andersen, T.B., Jamtveit, B., 1990. Uplift of deep crust during orogenic extensional collapse: a model based on field studies in the Sogn-Sunnfjord region of western Norway. Tectonics 9, 1097–1112.

Andersen, T.B., Berry, H.N., Lux, D.R., Andresen, A., 1998. The tectonic significance of pre-Scandian $^{40}Ar/^{39}Ar$ phengite cooling ages from the Caledonides of western Norway. Journal of the Geological Society of London 155, 297–309.

Anderson, M.W., Steltenpohl, M.G., Key, T.B., Andresen, A., Hames, W.E., 2010. Late-stage Caledonian collisional tectonics of northern Scandinavia: linked contractional and extensional exhumation of the Baltoscandian margin. Geological Society of America Abstracts with Programs 42 (5), 196.

Bartley, J.M., 1982. Limited basement involvement in Caledonian deformation, Hinnøy, North Norway, and tectonic implications. Tectonophysics 83, 185–203. doi:10.1016/0040-1951(82)90018-X.

Bartley, J.M., 1984. Caledonian structural geology and tectonics of east Hinnøy, north Norway. Norges Geologiske Undersøkelse 396, 1–24.

Bergh, S.G., Eig, K., Klovjan, O.S., Henningsen, T., Olesen, O., Hansen, J.A., 2007. The Lofoten-Vesteralen continental margin: a multiphase Mesozoic-Paleogene rifted shelf as shown by offshore-onshore brittle fault-fracture analysis. Norwegian Journal of Geology 87, 29–58.

Berry, H.N., Lux, D.R., Andresen, A., Andersen, T.B., 1995. Progressive exhumation during orogenic collapse as indicated by $^{40}Ar/^{39}Ar$ cooling ages from different structural levels, southwest Norway. Geonytt 22, 20–21.

Björklund, L.J.O., 1987. Basement-cover relationships and regional correlations of the Caledonian nappes, eastern Hinnøy, north Norway. Norsk Geologisk Tidsskrift 67, 3–14.

Blystad, P., Brekke, H., Færseth, R.B., Larsen, B.T., Skogseid, J., Tørudbakken, B., 1995. Structural elements of the Norwegian continental shelf II: the Norwegian Sea region. Norwegian Petroleum Directorate Bulletin 8, 1–45.

Braathen, A., 1999. Kinematics of polyphase brittle faulting in the Sunnfjord region, western Norway. Tectonophysics 302, 99–121.

Braathen, A., Osmundsen, P.T., Nordgulen, Ø, Roberts, D., Meyer, G.B., 2002. Orogen-parallel extension of the Caledonides in northern central Norway: and overview. Norwegian Journal of Geology 82, 225–241.

Brekke, H., 2000. The Tectonic Evolution of the Norwegian Seacintinental Margin with Emphasis on the Vøring and Møre Basins. In: Geological Society of London Special Publication, vol. 167, pp. 327–378.

Brekke, H., Riis, F., 1987. Tectonics and basin evolution of the Norwegian shelf between 62° and 72°N. Norsk Geologisk Tidsskrift 67, 295–322.
Brozzetti, F., Boncio, P., Lavecchia, G., Pace, B., 2009. Present activity and seismogenic potential of a low-angle normal fault system (Cita di Castello, Italy): constraints from surface geology, seismic reflection data and seismicity. Tectonophysics 463, 31–46.
Buatier, M., van Roermund, H.L.M., Drury, M., Lardeaux, J.M., 1991. Deformation and recrystallization mechanisms in naturally deformed omphacites from the Sesia-Lanzo zone; geophysical consequences. Tectonophysics 195, 11–27.
Bugge, T., Ringås, J.E., Leith, D.A., Mangerud, G., Weiss, H.M., Leith, T.L., 2002. Upper Permian as a new play model on the mid-Norwegian continental shelf: investigated by shallow stratigraphic drilling. American Association of Petroleum Geologists Bulletin 86, 107–127.
Coker, J.E., Steltenpohl, M.G., Andresen, A., Kunk, M.J., 1995. An $^{40}Ar/^{39}Ar$ thermochronology of the Ofoten-Troms region: implications for terrane amalgamation and extensional collapse of the northern Scandinavian Caledonides. Tectonics 14 (2), 435–447.
Corfu, F., 2004. U–Pb geochronology of the Leknes group: an exotic early-Caledonian metasedimentary assemblage stranded on Lofoten basement, northern Norway. Journal of the Geological Society of London 161, 619–627.
Dalland, A., 1975. The Mesozoic rocks of Andøy, northern Norway. Norges Geologiske Undersøkelse 316, 271–287.
Davids, C., Bergh, S., Wemmer, K., Layer, P., 2010. K–Ar and $^{40}Ar/^{39}Ar$ geochronology of post Caledonian extension in Vesterålen and Troms, northern Norway. In: Norges Geologisk Forening (Geological Society of Norway), Nordic Geologic Winter Meeting, Abstracts and Proceedings, vol. 1, p. 39.
Davidsen, B., Sommaruga, A., Bøe, R., 2001a. Final report: Sedimentation, tectonics and uplift in Vesterålen. Phase 1 – Localizing near-shore faults and Mesozoic sediment basins. Norges Geologiske Undersøkelse Report 2001.111. p. 16.
Davidsen, B., Smelor, M., Ottesen, D., 2001b. Et nyoppdaget Mesozoic basseng I Sortlandsundet, Vesterålen. Norsk Geologiske Foreningen, XVII Vinterkonferanse, Abstracts Volume, Trondheim, Norway, pp. 42–43.
Ebbing, J., Lundin, E., Olesen, O., Hansen, E.K., 2006. The mid-Norwegian margin: a discussion of crustal lineaments, mafic intrusions, and remnants of the Caledonian root by 3D density modeling and structural interpretation. Journal of the Geological Society of London 163, 47–59.
Eide, E.A., Osmundsen, P.T., Meyer, G.B., Kendrick, M.A., Corfu, F., 2002. The Nesna shear zone, north-central Norway: an $^{40}Ar/^{39}Ar$ record of Early Devonian-Early Carboniferous ductile extension. Norsk Geologisk Tiddskrift 82, 317–339.
Fleck, R.J., Sutter, J.F., Elliott, D.H., 1977. Interpretation of discordant $^{40}Ar/^{39}Ar$ age-spectra of Mesozoic tholeiites from Antarctica. Geochemica et Cosmochemica Acta 41, 15–32. doi:10.1016/0016-7037(77)90184-3.
Fossen, H., 1992. The role of extensional tectonics in the Caledonides of South Norway. Journal of Structural Geology 14, 1033–1046.
Fossen, H., 2010. Extensional tectonics in the North Atlantic Caledonides: a regional view. In: Law, R., Butler, R., Holdsworth, B., Krabbendam, R.A., Strachan, M. (Eds.), Continental Tectonics and Mountain Building: The Legacy of Peach and Horn. Geological Society of London Special Publication, vol. 335, pp. 767–793.
Fossen, H., Rykkelid, E., 1992. Postcollisional extension of the Caledonide orogen in Scandinavia: structural expressions and tectonic significance. Geology 20, 737–740.
Fossen, H., Rykkelid, E., 1993. Reply to comment on "Postcollisional extension of the Caledonide orogen in Scandinavia: structural expressions and tectonic significance". Geology 21, 477–478.
Fricke, H.C., Wickham, S.M., O'Neil, J.R., 1992. Oxygen and hydrogen isotope evidence for meteoric water infiltration during mylonitization and uplift in the Ruby Mountains-East Humboldt Range core complex, Nevada. Contributions to Mineralogy and Petrology 111, 203–221.
Griffin, W.L., Taylor, P.N., Hakkinen, J.W., Heier, K.S., Iden, I.K., Krogh, E.J., Malm, O., Olsen, K.I., Ormassen, D.E., Tveten, E., 1978. Archean and Proterozoic crustal evolution of Lofoten-Vesterålen, north Norway. Journal of the Geological Society of London 135, 629–647.
Hacker, B.R., McClelland, W.C., Liou, J.G. (Eds.), 2006. Ultrahigh-Pressure Metamorphism: Deep Continental Subduction. Geological Society of America Special Paper, vol. 403.
Hames, W.E., Andresen, A., 1996. Timing of orogeny and extension in the continental shelf of north-central Norway as indicated by laser $^{40}Ar/^{39}Ar$ muscovite dating. Geology 24 (11), 1005–1008.
Hansen, J.A., 2009. Onshore-Offshore tectonic relations on the Lofoten and Vesterålen margin: Mesozoic to early Cenozoic structural evolution and morphological implications. Ph.D. thesis, University of Tromsø, Tromsø, Norway.
Hartz, E., Andresen, A., 1995. Caledonian sole thrust of central East Greenland: a crustal-scale Devonian extensional detachment? Geology 23, 637–640.
Heier, K.S., 1960. Petrology and geochemistry of high-grade metamorphic and igneous rocks on Langøy, Northern Norway. Norges Geologiske Undersøkelse 207, 1–246.
Hendriks, B.W.H., Osmundsen, P.T., Redfield, T.F., 2010. Normal faulting and block tilting in Lofoten and Vesterålen constrained by apatite fission track data. Tectonophysics. doi:10.1016/j.tecto.2009.12.011.
Hodges, K.V., Bartley, J.M., Burchfiel, B.C., 1982. Structural evolution of an A-type subduction zone, Lofoten Rombak area, northern Scandinavian Caledonides. Tectonics 1, 441–462.
Key, T.B., 2010. Structure and Timing of the Austerfjord Thrust and Related Shear Zones, Hinnøy, North Norway: Implications for Late-stage Caledonian Tectonic Evolution. M.S. Thesis, Auburn University, Auburn, Alabama.
Key, T.B., Steltenpohl, M.G., Andresen, A., Ball, J.B., Hames, W.E., 2008. Field and petrographic investigation of the Austerfjord group, Austerfjord thrust, and Sørfjorden shear zone, Hinnøy, north Norway, implications for Caledonian tectonic evolution. Geological Society of America Abstracts with Programs 40 (6), 152.
Kerrich, R., Hyndman, D., 1986. Thermal and fluid regimes in the Bitterroot Lobe-Saphire Block detachment zone, Montana: evidence from $^{18}O/^{16}O$ and geologic relations. Geological Society of America Bulletin 97, 147–155.
Klein, A., Steltenpohl, M.G., 1999. Basement-cover relations and late- to post-Caledonian extension in the Leknes group, west-central Vestvagoy, Lofoten, north Norway. Norsk geologisk tidsskrift 79, 19–31.
Klein, A., Steltenpohl, M.G., Hames, W.E., Andresen, A., 1999. Ductile and brittle extension in the southern Lofoten archipelago, north Norway: implications for differences in tectonic style along an ancient collisional margin. American Journal of Science 299, 69–89.
Larsen, P.H., Olsen, H., Clark, J.A., 2008. The Devonian basin in East Greenland: review of basin evolution and vertebrate assemblages. In: Higgins, A.K., Gilotti, J.A., Smith, M.P. (Eds.), The Greenland Caledonides: Evolution of the Northeastern Margin of Laurentia. Geological Society of America Memoir, vol. 202, pp. 273–292.
Løseth, H., Tveten, E., 1996. Post-Caledonian structural evolution of the Lofoten and Vesteralen offshore and onshore areas. Norwegian Journal of Geology 76, 215–230.
Mager, S., 2005. The late- to post-Caledonian extensional history of northwest Hinnøy, North Norway. M.S. Thesis, Auburn University, Auburn, Alabama.
McDougall, I., Harrison, T.M., 1999. Geochronology and Thermochronology by the $Ar/^{39}Ar$ ^{40}Method. Oxford University Press, New York.
Mjelde, R., Kodaira, S., Sellevoll, M.A., 1996. Crustal structure of the Lofoten margin, N. Norway, from normal incidence and wide-angle seismic data: a review. Norsk Geologisk Tidsskrift 76, 187–198.
Moecher, D.P., Steltenpohl, M.G., 2009. Direct calculation of rupture depth for an exhumed paleoseismogenic fault from mylonitic pseudotachylyte. Geology 37, 999–1002.
Moecher, D.P., Steltenpohl, M.G. Petrologic Evidence for Co-Seismic Slip in Extending Middle to Lower Continental Crust: Heier's Zone of Pseudotachylyte, North Norway. In: Fagereng, Å., Toy, V. (Eds.), Geology of the Earthquake Source: A Volume in Honour of Rick Sibson. Geological Society of London Special Paper 542, in press.
Northrup, C.J., 1997. Timing structural assembly, metamorphism, and cooling of Caledonian nappes, Ofoten-Efjorden, north Norway: tectonic insights from U–Pb and $^{40}Ar/^{39}Ar$ geochronology. Journal of Geology 105, 565–582.
Olsen, H., 1993. Sedimentary basin analysis of the continental Devonian basin in north-east Greenland. Bulletin Grønlands Geologiske Undersøkelse 168.
Olesen, O., Lundin, E., Nordgulen, Ø, Osmundsen, P.T., Skilbrei, J.R., Smethurst, M.A., Solli, A., Bugge, T., Fichler, C., 2002. Bridging the gap between the onshore and offshore geology in Nordland, northern Norway. Norwegian Journal of Geology 82, 243–262.
Olesen, O., Torsvik, T.H., Tveten, E., Zwann, K.B., Løseth, H., Henningsen, T., 1997. Basement structure of the continental margin in the Lofoten Lopphavet area, northern Norway: constraints from potential field data, on-land structural mapping and palaeomagnetic data. Norsk Geologisk Tidsskrift 77, 15–30.
Osmundsen, P.T., Andersen, T.B., 1994. Caledonian compression and late-orogenic extensional deformation in the Staveneset area, Sunnifjord, Western Norway. Journal of Structural Geology 16, 1385–1401.
Osmundsen, P.T., Ebbing, J., 2008. Styles of extension offshore mid-Norway and implications for mechanisms of crustal thinning at passive margins. Tectonics 27. doi:10.1029/2007TC002242.
Osmundsen, P.T., Andersen, T.B., Markussen, S., Svendby, A.K., 1998. Tectonics and sedimentation in the hangingwall of a major extensional detachment: the Devonian Kvamshesten Basin, western Norway. Basin Research 10, 213–224.
Osmundsen, P.T., Braathen, A., Nordgulen, Ø, Roberts, D., Meyer, G.B., Eide, E., 2003. The Devonian Nesna shear zone and adjacent gneiss-cored culminations, North-Central Norwegian Caledonides. Journal of the Geological Society of London 160, 137–150.
Osmundsen, P.T., Redfield, T.F., Hendriks, B.H.W., Bergh, S., Hansen, J.-A., Henderson, I.H.C., Dehls, J., Lauknes, T.R., Larsen, Y., Anda, E., Davidsen, B., 2010. Fault-controlled alpine topography in Norway. Journal of the Geological Society of London 167, 83–98. doi:10.1144/0016-76492009-019.
Osmundsen, P.T., Sommaruga, A., Reider, Skillbrei, J.R, Olesen, O., 2002. Deep structure of the mid-Norway rifted margin. Norwegian Journal of Geology 82, 205–224.
Passchier, C.W., Trouw, R.A.J., 1996. Microtectonics. Springer, Berlin.
Plattner, U., Markl, G., Sherlock, S., 2003. Chemical heterogeneities of Caledonian (?) pseudotachylytes in the Eidsfjord anorthosite, north Norway. Contributions to Mineralogy and Petrology 145, 316–338.
Roberts, D., 2003. The Scandinavian Caledonides: event chronology, palaeogeographic settings and likely modern analogues. Tectonophysics 365, 283–299. doi:10.1016/S0040-1951(03)00026-X.
Rykkelid, E., 1992. Basement deformation in the northern Scandinavian Caledonides. Ph.D. thesis, University of Oslo, Oslo, Norway.
Rykkelid, E., Andresen, A., 1994. Late Caledonian extension in the Ofoten area, northern Norway. Tectonophysics 231, 157–169.
Sherlock, S.C., 2001. Two-stage erosion and deposition in a continental margin setting: an $^{40}Ar/^{39}Ar$ laserprobe study of offshore detrital white micas in the Norwegian Sea. Journal of the Geological Society of London 158 (5), 793–799. doi:10.1144/0016-764001-021.

Sibson, R.H., 1975. Generation of pseudotachylyte by ancient seismic faulting. Geophysical Journal of the Royal Astronomical Society 43, 775–794.
Steltenpohl, M.G., Bartley, J.M., 1988. The tectonic significance of crossfolds and backfolds in the Norwegian Caledonides. Geological Society of America Bulletin 100, 140–151.
Steltenpohl, M.G., Bartley, J.M., 1993. Comment on "Postcollisional extension of the Caledonide orogen in Scandinavia: structural expressions and tectonic significance. Geology 21, 476–477.
Steltenpohl, M.G., Hames, W.E., Andresen, A., 2004. The Silurian to Permian history of a metamorphic core complex in Lofoten, northern Scandinavian Caledonides. Tectonics 23, 1–23. doi:10.1029/2003TC001522. TC1002.
Steltenpohl, M.G., Kassos, G., Andresen, A., 2006. Retrograded eclogite-facies pseudotachylites as deep-crustal paleoseismic faults within continental basement of Lofoten, north Norway. Geosphere 2 (1), 61–72. doi:10.1130/GES00035.1.
Steltenpohl, M.G., Carter, B.T., Andresen, A., Zeltner, D.L., 2009. $^{40}Ar/^{39}Ar$ thermochronology of late- and postorogenic extension in the Caledonides of north-central Norway. Journal of Geology 117, 399–414. doi:10.1086/599217.
Steltenpohl, M.G., Hames, W.E., Andresen, A., Markl, G., 2003a. A new Caledonian eclogite province in Norway and potential Laurentian (Taconic) and Baltic links. Geology 31 (11), 985–988. doi:10.1130/G19744.1.
Steltenpohl, M.G., Andresen, A., Lindstrom, M., Gromet, P., Steltenpohl, L.W., 2003b. The role of felsic and mafic igneous rocks in deciphering the evolution of thrust-stacked terranes: an example from the north Norwegian Caledonides. American Journal of Science 303, 149–185.
Steltenpohl, M.G., Ball, J.B., Moecher, D.P., Andresen, A., 2010a. The Eidsfjord Detachment: an Early Devonian, Paleoseismogenic Low-angle Normal Detachment Fault Exposed in Lofoten-Vesterålen, North Norway. In: Norges Geologisk Forening (Geological Society of Norway), Nordic Geologic Winter Meeting, Abstracts and Proceedings, vol. 1, pp. 186–189.
Steltenpohl, M.G., Hames, W.E., Key, T.B., Ball, J.B., Kassos, G., Andresen, A., Tveten, E., Bream, B.R., Braun, S.A., Rehnström, E.F., 2010b. The western half of the Ofoten-Lofoten transect. In: Norges Geologisk Forening (Geological Society of Norway), Nordic Geologic Winter Meeting, Abstracts and Proceedings, vol. 1, p. 186.
Steltenpohl, M.G., Kassos, G., Andresen, A., Rehnström, E.F., Hames, W.E., 2011. Eclogitization and exhumation of Caledonian continental basement in Lofoten, North Norway. Geosphere 7 (1), 1–17. doi:10.1130/GES00573.1.
Stemmerik, L., Christiansen, F.G., Piasecki, S., Jordt, B., Marcussen, C., Nøhr-Hansen, H., 1993. Depositional history and petroleum geology of the Carboniferous to Cretaceous sediments in the northern part of East Greenland. In: Vorren, T.O., et al. (Eds.), Arctic Geology and Petroleum Potential. Norwegian Petroleum Society Special Publication, vol. 2, pp. 67–87.
Stephens, M.B., Kullerud, K., Claesson, S., 1993. Early Caledonian tectonothermal evolution in outboard terranes, central Scandinavian Caledonides: new constraints from U–Pb zircon dates. Journal of the Geological Society of London 150, 51–56.
Tsikalas, F., Eldholm, O., Faleide, J.I., 2005. Crustal structure of the Lofoten-Vesterålen continental margin off Norway. Tectonophysics 404, 151–174.
Tsikalas, F., Faleide, J.I., Eldholm, O., 2001. Lateral variations in tectono-magmatic style along the Lofoten-Vesterålen volcanic margin off Norway. Marine and Petroleum Geology 18, 807–832.
Tsikalas, F., Faleide, J.I., Kusznir, N.J., 2008. Along-strike variations in rifted margin crustal architecture and lithosphere thinning between northern Vøring and Lofoten margin segments off mid-Norway. Tectonophysics 458, 68–81. doi:10.1016/j.tecto.2008.03.001.
Tull, J.F., 1978. Geology and structure of Vestvågøy, Lofoten, north Norway. Norges Geologiske Undersøkelse 42.
Tullis, J.A., 1983. Deformation of feldspars. In: Ribbe, P.H. (Ed.), Feldspar Mineralogy. Mineralogical Society of America Short Course Notes, vol. 2, pp. 297–323.
Tveten, E., 1978. Svolvaer, berggrunnskart 1:250000. Norges Geologiske Undersøkelse, Norges Geologisk Berggrunnskart over Norge, scale 1:1,000,000.
Voll, G., 1976. Recrystallization of quartz, biotite, and feldspars from Erstfeld in the Levantina nappe, Swiss Alps, and geological implications. Schweizerische Mineralogische und Petrographische Mitteilungen 56, 641–647.
Walsh, E.O., Hacker, B.R., Gans, P.B., Grove, M., Gehrels, G., 2007. Protolith ages and exhumation histories of (ultra)high-pressure rocks across the Western Gneiss Region, Norway. Geological Society of America Bulletin 119, 289–301.
Wilson, R.W., McCaffrey, K.J.W., Holdsworth, R.E., Jones, R.R., Imber, J., Clegg, P., 2005. Lofoten has its faults! Detailed fault analysis and 3D digital mapping in Norway's Lofoten Islands. Geoscientist 15.
Wilson, R.W., McCaffrey, K.J.W., Holdsworth, R.E., Imber, J., Jones, R., Welbon, A., Roberts, D.J., 2006. Complex fault patterns, transtension, and structural segmentation of the Lofoten Ridge, Norwegian Margin: using digital mapping to link onshore and offshore geology. Tectonics 25 TC4018.